Diffusion Synthetic Acceleration of Discontinuous Finite Element Transport Iterations

Marvin L. Adams & William R. Martin

Diffusion Synthetic Acceleration of Discontinuous Finite Element Transport Iterations

Marvin L. Adams*

Lawrence Livermore National Laboratory, P.O. Box 808, L-18, Livermore, California 94550

and

William R. Martin

The University of Michigan, Department of Nuclear Engineering, Ann Arbor, Michigan 48109

Abstract — *We present a discretization of the diffusion equation that can be used to accelerate transport iterations when the transport equation is spatially differenced by a discontinuous finite element (DFE) method. That is, we present a prescription for diffusion synthetic acceleration of DFE transport iterations. (The well-known linear discontinuous and bilinear discontinuous schemes are examples of DFE transport differencings.) We demonstrate that our diffusion discretization can be obtained in any coordinate system on any grid. We show that our diffusion discretization is not strictly consistent with the transport discretization in the usual sense. Nevertheless, we find that it yields a scheme with unconditional stability and rapid convergence. Further, we find that as the optical thickness of spatial cells becomes large, the spectral radius of the iteration scheme approaches zero (i.e., instant convergence). We give analysis results for one- and two-dimensional Cartesian geometries and numerical results for one-dimensional Cartesian and spherical geometries.*

I. INTRODUCTION

A considerable volume of work has been reported recently on diffusion synthetic acceleration (DSA) of transport iterations (see Refs. 1 through 6 and references therein). A full DSA iteration involves a fixed-source transport calculation, followed by a diffusion calculation designed to improve the transport result. It has long been known that the success of a DSA scheme depends sensitively on the discretizations of the transport and diffusion equations[1,2,7]; in particular, the most successful schemes have employed diffusion discretizations that are closely related to the transport discretizations being accelerated.[1-3]

We present here a discontinuous finite element (DFE) diffusion discretization that we use to acceler-

ate DFE transport iterations.[8,9] We show that we can derive our diffusion discretization in any coordinate system on any spatial grid (including unstructured, arbitrarily connected grids). Our first main result is that our discretization produces an unconditionally stable and rapidly convergent DSA scheme. Our second main result is that the spectral radius of our DSA scheme tends to zero (immediate convergence) as spatial cells become optically thick. (We believe these results hold in general, but we can prove them only for problems we have analyzed or tested.) Our results are obtained by Fourier analyses[2] of idealized model problems in one- and two-dimensional Cartesian geometries and by numerical testing in one-dimensional Cartesian and spherical geometries.

The unconditional rapid convergence of our DSA scheme demonstrates that a DSA method can succeed even with a diffusion discretization that is not "consistent" with the given transport discretization. (We define "consistent" later.) This should help to answer an

---

important question: What properties must a DSA diffusion discretization possess for the DSA scheme to be effective? Previous research indicates that consistency is a sufficient property; however, consistent diffusion discretizations can be algebraically complicated and potentially difficult to solve. Thus, the freedom to be "inconsistent" (and simpler) could lead to more efficient DSA algorithms.

Our scheme approaches immediate convergence as the spatial cells in a problem become optically thick. From an academic point of view, we find it very interesting that such behavior is possible. From a practical point of view, this behavior could be quite significant in certain applications, most notably radiative transfer.

In Sec. II, we provide an introductory description of DSA. We discuss some previous DSA research, emphasizing results that motivated this work. In Sec. III, we specify exactly what we mean by DFE transport. In Sec. IV, we present our DFE diffusion discretization for a very general case: an arbitrarily connected grid in Cartesian geometry. For reasons that we discuss later, we give two distinct derivations of our scheme. In the first derivation, we obtain a DFE diffusion equation from the *analytic diffusion equation*; in the second, we obtain a DFE diffusion equation from the *DFE transport equation*. Interestingly, our two derivations lead to exactly the same DFE diffusion equations. In Sec. V, we present Fourier analyses of model problems, and in Sec. VI, we give numerical results from several test problems. In Sec. VII, we summarize our results and discuss their significance.

To illustrate that curvilinear geometries are treated in the same way as Cartesian geometries, we include in Appendix A a derivation of our linear discontinuous diffusion discretization in spherical geometry. To illustrate our DFE equation in two dimensions, we give in Appendix B our bilinear DFE diffusion discretization for rectangular spatial cells in x-y geometry. Finally, in Appendix C we demonstrate that our linear DFE diffusion equations in slab geometry can be cast as a tridiagonal system for either cell-averaged or cell-edge unknowns.

II. BACKGROUND: DIFFUSION SYNTHETIC ACCELERATION

We open this section by describing diffusion synthetic acceleration (DSA) applied to an analytic (not discretized) transport problem with one energy group and with isotropic scattering. We begin with the equations for a very simple iteration scheme known as "source iteration":

$$\mathbf{\Omega} \cdot \nabla \Psi^{(l+1/2)} + \sigma_t(r) \Psi^{(l+1/2)}(r, \mathbf{\Omega})$$

$$= \frac{\sigma_s(r)}{4\pi} \Phi_0^{(l)}(r) + q(r, \mathbf{\Omega}) \qquad (1)$$

and

$$\Phi_0^{(l+1)}(r) = \Phi_0^{(l+1/2)}(r) \equiv \int_{4\pi} d\Omega \, \Psi^{(l+1/2)}(r, \mathbf{\Omega}) \, ,$$

$$(2)$$

where

r = position

$\mathbf{\Omega}$ = unit vector in the direction of particle travel

Ψ = angular flux

Φ = scalar flux

σ_t = total cross section

σ_s = scattering cross section

q = angular source rate density.

The first step of source iteration, given by Eq. (1), is to calculate the angular flux Ψ given a guess for the scalar flux Φ. We call this a "transport sweep." The second step, given by Eq. (2), is to form a new scalar flux by integrating the angular flux over angle. It is easy to show[2] that this iteration scheme converges very slowly for problems in which particles are likely to undergo a large number of scattering collisions before they "die" via leakage or absorption. Because many problems of practical interest have this property, we are very interested in iteration schemes that converge faster than source iteration. DSA is one such scheme.

A DSA iteration also involves a transport sweep, Eq. (1), but uses a diffusion solution to obtain the new scalar flux. We shall derive DSA here using a four-step procedure that was first presented by Larsen.[2] In step 1, we take zeroth and first angular moments of Eq. (1), obtaining

$$\nabla \cdot \Phi_1^{(l+1/2)} + \sigma_t(r)\Phi_0^{(l+1/2)}(r)$$

$$= \sigma_s(r)\Phi_0^{(l)}(r) + q_0(r) \qquad (3a)$$

and

$$\tfrac{1}{3}\nabla \Phi_0^{(l+1/2)} + \tfrac{2}{3}\nabla \cdot \Phi_2^{(l+1/2)} + \sigma_t(r)\Phi_1^{(l+1/2)}(r)$$

$$= q_1(r) \, , \qquad (3b)$$

where

$$\Phi_1^{(l+1/2)}(r) = \text{``current''} = \int_{4\pi} d\Omega \, \mathbf{\Omega}\Psi^{(l+1/2)}(r, \mathbf{\Omega}) \, ,$$

$$\Phi_2^{(l+1/2)}(r) = \text{``second-moment tensor''}$$

$$= \int_{4\pi} d\Omega \, \frac{1}{2} \, (3\mathbf{\Omega}_m\mathbf{\Omega}_m - 1)\Psi^{(l+1/2)}(r, \mathbf{\Omega}) \, ,$$

$$q_0(r) = \int_{4\pi} d\Omega \, q(r, \mathbf{\Omega}) \, ,$$

and

$$q_1(r) = \int_{4\pi} d\Omega\, \Omega q(r,\Omega) \ .$$

In step 1 we have not changed anything; we have simply obtained some equations that are satisfied at the end of each transport sweep.

In step 2, we define "acceleration equations" that will determine our end-of-iteration scalar flux and current. In this step, we rewrite Eqs. (3) with some of the iteration indices changed to $(l + 1)$:

$$\nabla \cdot \Phi_1^{(l+1)} + \sigma_t(r)\Phi_0^{(l+1)}(r) = \sigma_s(r)\Phi_0^{(l+1)}(r) + q_0(r)$$

$$\tag{4a}$$

and

$$\tfrac{1}{3}\nabla\Phi_0^{(l+1)} + \tfrac{2}{3}\nabla \cdot \Phi_2^{(l+1/2)} + \sigma_t(r)\Phi_1^{(l+1)}(r) = q_1(r) \ .$$

$$\tag{4b}$$

We emphasize two things about these "acceleration equations." First, they are a coupled set of equations that completely determine the end-of-iteration scalar flux $\Phi_0^{(l+1)}$ and current $\Phi_1^{(l+1)}$. Second, Eq. (4a) is a statement of conservation or "balance"; thus, the end-of-iteration scalar flux and current will satisfy the balance equation. It has long been recognized that forcing balance at the end of each iteration can accelerate transport iterations.[7] This observation helps us understand why DSA succeeds.

Step 3 is simply algebra; we subtract Eqs. (3) from Eqs. (4) and rearrange:

$$\nabla \cdot F_1^{(l+1)} + \sigma_a(r)F_0^{(l+1)}(r)$$

$$= \sigma_s(r)\,[\Phi_0^{(l+1/2)}(r) - \Phi_0^{(l)}(r)] \tag{5a}$$

and

$$\tfrac{1}{3}\nabla F_0^{(l+1)} + \sigma_t(r)F_1^{(l+1)}(r) = 0 \ , \tag{5b}$$

where we have defined

$$F_0^{(l+1)}(r) \equiv \Phi_0^{(l+1)}(r) - \Phi_0^{(l+1/2)}(r) \ ,$$

$$F_1^{(l+1)}(r) \equiv \Phi_1^{(l+1)}(r) - \Phi_1^{(l+1/2)}(r) \ ,$$

and

$$\sigma_a(r) \equiv \sigma_t(r) - \sigma_s(r) \ .$$

Step 4 is more algebra: We eliminate the current vector F_1 from this system to produce a diffusion equation for the scalar flux correction F_0:

$$-\nabla \cdot \frac{1}{3\sigma_t(r)} \nabla F_0^{(l+1)} + \sigma_a(r)F_0^{(l+1)}(r)$$

$$= \sigma_s(r)\,[\Phi_0^{(l+1/2)}(r) - \Phi_0^{(l)}(r)] \ . \tag{6}$$

The complete DSA iteration scheme is therefore given by

$$\Omega \cdot \nabla \Psi^{(l+1/2)} + \sigma_t(r)\Psi^{(l+1/2)}(r,\Omega)$$

$$= \frac{\sigma_s(r)}{4\pi} \Phi_0^{(l)}(r) + q(r,\Omega) \ , \tag{7a}$$

$$\Phi_0^{(l+1/2)}(r) \equiv \int_{4\pi} d\Omega\, \Psi^{(l+1/2)}(r,\Omega) \ , \tag{7b}$$

and

$$-\nabla \cdot \frac{1}{3\sigma_t(r)} \nabla F_0^{(l+1)} + \sigma_a(r)F_0^{(l+1)}(r)$$

$$= \sigma_s(r)\,[\Phi_0^{(l+1/2)}(r) - \Phi_0^{(l)}(r)] \ , \tag{8a}$$

$$\Phi_0^{(l+1)}(r) = \Phi_0^{(l+1/2)}(r) + F_0^{(l+1)}(r) \ . \tag{8b}$$

It is easy to show that this DSA scheme converges very rapidly, at least for problems we can analyze.[2]

At this point, we have discussed only analytic, not discretized, equations. In practice, we must discretize our transport equation if we are to solve practical problems. Early DSA researchers found that after discretization, Eqs. (7) and (8) produced iteration schemes that were unstable.[7] Alcouffe overcame this problem when he realized that the discretization of the diffusion equation, Eq. (8a), must be intimately related to the discretization of the transport equation, Eq. (7a). Using this insight, he developed discretizations of the diffusion equation, Eq. (8a), that yield stable and effective DSA schemes when the transport equation, Eq. (7a), is discretized by the diamond-differencing method.[1] Larsen subsequently devised a procedure for obtaining a consistent discretization of the diffusion equation for virtually any given transport discretization. He showed that the resulting DSA scheme, which we call "standard linear DSA," is rapidly convergent for all transport discretizations that were tested.[2] Larsen's procedure is exactly the four-step derivation of DSA that is outlined above, except that it begins with the *discretized* version of the transport equation (1) and produces a *discretized* version of Eqs. (5). Thus, the diffusion discretization of standard linear DSA is completely *consistent* with the underlying transport discretization. The prevailing wisdom among researchers at that time was that complete consistency was probably the only way to guarantee stable and effective DSA methods.

We note that in general, the standard linear DSA discretization of Eqs. (5) is algebraically complicated and potentially difficult to solve.[2] In particular, it may not be possible to eliminate the current vectors from the discretized version of Eqs. (5) in general multidimensional problems. This complexity has precluded any widespread use of standard linear DSA to date. Thus, there is a need for simpler diffusion discretizations that produce stable, rapidly convergent DSA algorithms. That is, we need simple "nonstandard" DSA methods that work.

In an effort to achieve this, Khalil[3] has devised a

relatively simple procedure for obtaining discretized diffusion equations for DSA. This procedure is applicable to a class of transport discretizations known as "nodal methods." Given a particular nodal transport discretization, Khalil carefully notes the approximations that were used to derive it from the analytic transport equation. He then derives a diffusion discretization by applying similar approximations to the *analytic diffusion* equation. This is in contrast to standard linear DSA, which derives its discrete diffusion equation directly from the *discrete transport* equation. We graphically depict these two different procedures in Fig. 1.

It is not at all obvious that Khalil's procedure and standard linear DSA will produce similar diffusion discretizations. The two paths shown in Fig. 1 simply do not have to arrive at the same point. In particular, the path taken by Khalil involves very little algebraic complexity, whereas the path of standard linear DSA involves considerable algebraic complexity. Despite this, Khalil[3] has shown that, at least in slab geometry, his diffusion differencings are almost equivalent to those of standard linear DSA. (Whether this is true in two or three dimensions remains unclear.) Khalil has also shown that his diffusion discretizations produce stable and rapidly convergent DSA schemes.[3]

To summarize, we have briefly discussed DSA for analytic (not discretized) transport iterations. We have also discussed three different DSA procedures that are stable and effective for discretized transport iterations. Two of these, standard linear DSA and Alcouffe's diamond-differencing DSA, use diffusion discretizations that are strictly consistent with their underlying transport discretizations. The third, Khalil's DSA, uses diffusion discretizations that appear to be *almost* consistent with its underlying transport discretizations. In contrast, the DFE diffusion discretizations that we present in this work are *not* consistent with DFE transport discretizations, nor are they nearly so. Despite this, we shall show that our discretizations produce unconditionally stable and rapidly convergent acceleration methods for DFE transport iterations.

III. DISCONTINUOUS FINITE ELEMENT TRANSPORT

In this section, we derive a generic DFE transport discretization, thus clarifying the class of transport discretizations that we are addressing. We then illustrate this class of schemes by giving the equations for the linear DFE method in slab geometry.

III.A. Discontinuous Finite Element Transport: General Cartesian Geometry

In this subsection, we derive a family of DFE spatial discretizations for the transport equation. We assume isotropic scattering and Cartesian geometry, and we allow the spatial grid to be arbitrary. Given a single energy group, the discrete ordinates transport equation under these assumptions is

$$\Omega_m \cdot \nabla \Psi_m + \sigma_t(r)\Psi_m(r)$$
$$= \sigma_s(r)\Phi_0(r) + q_m(r) \ , \quad r \in \partial D \qquad (9a)$$

and

$$\Phi_0(r) = \sum_{m=1}^{M} w_m \Psi_m(r) \ , \qquad (9b)$$

where

$\Psi_m(r)$ = angular flux at position r in direction Ω_m

$q_m(r)$ = source at position r in direction Ω_m
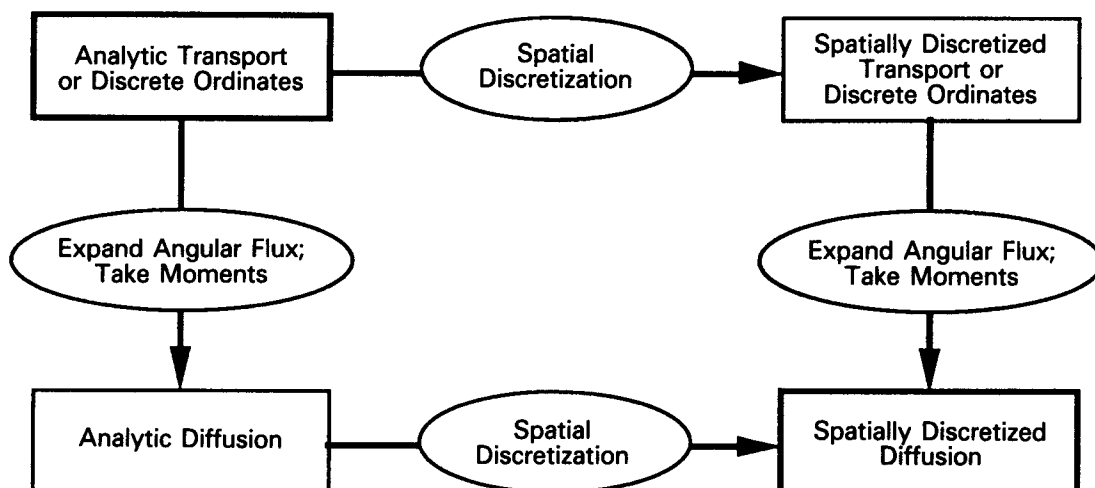
D = spatial domain

m = direction index

Fig. 1. Two paths leading from analytic transport to discrete diffusion.

and the quadrature weights w_m sum to unity. We shall treat the following boundary condition:

$$\Psi_m(r) = \beta(r)\Psi_m^{inc}(r) + [1 - \beta(r)]\Psi_m^{ref}(r) \ ,$$

$$r \in \partial D, \ n \cdot \Omega_m < 0 \ , \quad (9c)$$

where

Ψ_m^{inc} = specified incident angular flux

$\Psi_m^{ref}(r)$ = outgoing angular flux evaluated at the angle that would reflect onto angle Ω_m

n = unit outward normal at r.

At a given point r, we assume that either $\beta = 1$ (specified incident angular flux) or $\beta = 0$ (reflecting).

We assume that a grid has been placed on the problem domain D, dividing it into subdomains called zones, which we denote Z_k, $1 \leq k \leq K$. Within the k'th zone, we choose a set of weight functions $\{v_{ki}(r), 1 \leq i \leq J_k\}$ and a set of basis functions $\{b_{kj}(r), 1 \leq j \leq J_k\}$. The weight and basis functions are assumed to be continuous within each zone but may be discontinuous at zone surfaces. The weight and basis functions associated with a given zone are assumed to vanish outside that zone. With these assumptions, the DFE transport scheme can be obtained via the following three steps:

1. Multiply the discrete ordinates equation by a weight function $v_{ki}(r)$ and integrate over the k'th zone volume. Use Green's theorem on the leakage term, producing a zone-surface integral. Separate this surface integral into "incoming" and "outgoing" parts. The result is

$$\int_{[incoming \, \partial Z_k]_m} d^2r \, v_{ki}(r)n_k(r) \cdot \Omega_m \Psi_m(r)$$

$$+ \int_{[outgoing \, \partial Z_k]_m} d^2r \, v_{ki}(r)n_k(r) \cdot \Omega_m \Psi_m(r)$$

$$+ \int_{Z_k} d^3r(-\Psi_m\Omega_m \cdot \nabla v_{ki} + v_{ki}\sigma_t\Psi_m)$$

$$= \int_{Z_k} d^3r \, v_{ki}(\sigma_s\Phi_0 + q_m) \ ,$$

$$1 \leq i \leq J_k, \ 1 \leq k \leq K \ , \quad (10)$$

where

$n_k(r)$ = outward unit normal at point r on zone surface ∂Z_k

$[incoming \, \partial Z_k]_m$ = subset of k'th zone surface on which $n_k(r) \cdot \Omega_m < 0$

$[outgoing \, \partial Z_k]_m$ = subset of k'th zone surface on which $n_k(r) \cdot \Omega_m > 0$.

2. Replace quantities on zone surfaces (where they can be discontinuous) with their upstream values:

$[\Psi_m(r)]$ is replaced by

$$\begin{cases} \Psi_m(r_k^+) \ , & \text{for } r \text{ on } [incoming \, \partial Z_k]_m \\ \Psi_m(r_k^-) \ , & \text{for } r \text{ on } [outgoing \, \partial Z_k]_m \ , \end{cases} \quad (11)$$

where

$$r_k^+ = \lim_{\epsilon \to 0^+} (r + \epsilon n_k) \quad \text{for } r \text{ on } \partial Z_k$$

and

$$r_k^- = \lim_{\epsilon \to 0^+} (r - \epsilon n_k) \quad \text{for } r \text{ on } \partial Z_k \ .$$

That is, r_k^+ is just outside zone k, while r_k^- is just inside zone k. We use Ψ just outside the zone at incoming points and just inside the zone at outgoing points. (That is what we mean by "upstream.")

3. Approximate the unknowns as expansions in basis functions:

$$\Psi_m(r) \approx \psi_m(r) \equiv \sum_{k=1}^{K} \sum_{j=1}^{J_k} \psi_{mkj}b_{kj}(r) \quad (12a)$$

and

$$\Phi_0(r) \approx \phi_0(r) \equiv \sum_{k=1}^{K} \sum_{j=1}^{J_k} \phi_{0kj}b_{kj}(r) \ . \quad (12b)$$

After these manipulations, Eq. (2) becomes

$$\int_{[incoming \, \partial Z_k]_m} d^2r \, v_{ki}(r)n_k(r) \cdot \Omega_m \psi_m(r_k^+)$$

$$+ \int_{[outgoing \, \partial Z_k]_m} d^2r \, v_{ki}(r)n_k(r) \cdot \Omega_m \psi_m(r_k^-)$$

$$+ \int_{Z_k} d^3r(-\psi_m\Omega_m \cdot \nabla v_{ki} + v_{ki}\sigma_t\psi_m)$$

$$= \int_{Z_k} d^3r \, v_{ki}(\sigma_s\phi_0 + q_m) \ ,$$

$$1 \leq i \leq J_k, \ 1 \leq k \leq K \ . \quad (13a)$$

[We emphasize that ψ and ϕ in this equation are our *approximate* solutions, as defined in Eqs. (12).] This equation defines a general DFE transport discretization on an arbitrary grid in Cartesian geometry. We note that the boundary condition, Eq. (9c), is incorporated[10] "naturally" into Eq. (13a) because we define

$$\psi_m(r_k^+) \equiv \beta(r_k)\psi_m^{inc}(r_k) + [1 - \beta(r_k)]\psi_m^{ref}(r_k) \ ,$$

$$r_k \in \partial D, \ n \cdot \Omega_m < 0 \ . \quad (13b)$$

The continuity of the angular flux at cell interfaces is also incorporated naturally in system (13) because of definition (11).

Equations (13) define a family of DFE transport discretizations. These very general equations hold on

any spatial grid in one, two, or three dimensions. In Sec. III.B, we rewrite these equations in more conventional notation for one specific member of the DFE family.

III.B. Linear Discontinuous Finite Elements, Slab Geometry

We illustrate here the generic DFE transport equations using the simple case of the linear DFE method in slab geometry. In this case, we define

$$v_{k1}(x) = b_{k1}(x) = \begin{cases} 1.0 , & x \in (x_{k-1/2}, x_{k+1/2}) \\ 0 , & \text{otherwise} , \end{cases}$$

$$v_{k2}(x) = b_{k2}(x)$$

$$= \begin{cases} \dfrac{2(x - x_k)}{h_k} , & x \in (x_{k-1/2}, x_{k+1/2}) \\ 0 , & \text{otherwise} , \end{cases}$$

$$h_k = x_{k+1/2} - x_{k-1/2} ,$$

$$x_k = \tfrac{1}{2}(x_{k+1/2} + x_{k-1/2}) ,$$

$$\mu_m = e_x \cdot \Omega_m = x \text{ component of } \Omega_m ,$$

and

$$\psi_m(x) = \psi_{mk} + \psi_{mk}^x \frac{2(x - x_k)}{h_k} ,$$

$$x \in (x_{k-1/2}, x_{k+1/2}) .$$

We assume that the angular flux is specified at the left boundary ($x = x_{1/2}$) and that the right boundary ($x = x_{K+1/2}$) is reflecting. We find then that Eqs. (13), with iteration indices inserted, become

$$\left[\frac{\mu_m}{h_k} (\psi_{m,k+1/2} - \psi_{m,k-1/2}) + \sigma_{tk}\psi_{mk} \right]^{(l+1/2)}$$

$$= \sigma_{sk}\phi_{0k}^{(l)} + q_{mk} , \tag{14a}$$

$$\left[\frac{3\mu_m}{h_k} (\psi_{m,k+1/2} + \psi_{m,k-1/2} - 2\psi_{mk}) + \sigma_{tk}\psi_{mk}^x \right]^{(l+1/2)}$$

$$= \sigma_{sk}\phi_{0k}^{x(l+1/2)} + q_{mk}^x , \tag{14b}$$

$$\phi_{0k}^{(l+1/2)} = \sum_{m=1}^{M} w_m \psi_{mk}^{(l+1/2)} , $$

and

$$\phi_{0k}^{x(l+1/2)} = \sum_{m=1}^{M} w_m \psi_{mk}^{x(l+1/2)} , \tag{14c}$$

where

$$\psi_{m,k+1/2}$$

$$\equiv \begin{cases} \psi_{mk} + \psi_{mk}^x , & \mu_m > 0 \text{ and } k > 0 , \\ \psi_{m,k+1} - \psi_{m,k+1}^x , & \\ & \mu_m < 0 \text{ and } k < K , \\ \psi_m^{inc} , & \mu_m > 0 \text{ and } k = 0 , \\ \psi_{n,k+1/2} , & -\mu_n = \mu_m < 0 \text{ and } k = K . \end{cases} \tag{14d}$$

Equations (14) illustrate linear DFE transport in one-dimensional Cartesian coordinates. In Appendix A, we illustrate DFE transport in curvilinear geometries, using the simple case of linear DFE in one-dimensional spherical geometry. In Appendix B, we illustrate DFE transport in two dimensions, using the bilinear DFE method for rectangular spatial cells in x-y geometry.

IV. DISCONTINUOUS FINITE ELEMENT DIFFUSION

Diffusion synthetic acceleration of practical transport calculations involves discretized transport and diffusion equations. As we discussed in Sec. II, the performance of DSA depends sensitively on the discretization scheme chosen for the diffusion equation. We present here a DFE discretization of the diffusion equation, Eq. (8a), that can be used when the transport equation, Eq. (7a), is discretized by a DFE method. We actually give two distinct derivations of DFE diffusion. The first begins with the *analytic diffusion* equation and mimics the derivation of DFE transport from the analytic transport equation. This derivation, which is very simple algebraically, corresponds to the lower-left path in Fig. 1. The second derivation begins with the *DFE transport* equation and uses a modified version of the standard linear DSA procedure to obtain DFE diffusion. This derivation, which illustrates the connection between our method and standard linear DSA, corresponds to the upper-right path in Fig. 1. Remarkably, the two derivations produce identical diffusion discretizations.

IV.A. First Derivation of Discontinuous Finite Element Diffusion

We begin in this subsection with the analytic diffusion equation, Eq. (8a), and apply the same steps that we used in Sec. III to derive DFE transport. Again, this derivation corresponds to the lower-left path shown in Fig. 1.

1. Multiply the diffusion equation by a weight function $v_{ki}(r)$, and integrate over the k'th zone volume. Use Green's theorem on the leakage term, producing a zone-surface integral. The result is

$$\int_{\partial Z_k} d^2r \, v_{ki}(r) n_k(r) \cdot [-D(r)\nabla F_0(r)]$$

$$+ \int_{Z_k} d^3r \, [D\nabla F_0 \cdot \nabla v_{ki} + v_{ki}(r)\sigma_a(r)F_0(r)]$$

$$= \int_{Z_k} d^3r \, v_{ki}(r)\sigma_s(r) \, [\Phi_0^{(l+1/2)}(r) - \Phi_0^{(l)}(r)] \ ,$$

$$1 \le i \le J_k, \ 1 \le k \le K \ . \quad (15)$$

2. The second step in the DFE transport derivation is to replace quantities on zone surfaces (where they can be discontinuous) with their upstream values. This makes sense with the transport equation, but here the quantity of interest is a net current, for which "upstream" is not well defined. However, we can eliminate the net current in favor of partial currents, for which "upstream" is well defined, and then use the upstream value for each partial current. We therefore rewrite the net current as follows:

$n_k(r) \cdot (-D\nabla F_0)_r$ = net current out of zone k
   at r on ∂Z_k ,

   = (outgoing partial current)

   − (incoming partial current)

   = $(\alpha F_0 - \frac{1}{2}n \cdot D\nabla F_0)_r$

   − $(\alpha F_0 + \frac{1}{2}n \cdot D\nabla F_0)_r$;

and then make the following replacement:

$n_k(r) \cdot (-D\nabla F_0)_r$ is replaced by

$$(\alpha F_0 - \frac{1}{2}n \cdot D\nabla F_0)_{r_k^-}$$
$$- (\alpha F_0 + \frac{1}{2}n \cdot D\nabla F_0)_{r_k^+} \ . \quad (16)$$

That is, we evaluate the incoming partial current just outside the zone and the outgoing partial current just inside the zone.

3. Approximate the unknowns as expansions in terms of the basis functions:

$$F_0(r) \approx f_0(r) \equiv \sum_{k=1}^{K} \sum_{j=1}^{J_k} f_{0kj} b_{kj}(r) \ . \quad (17)$$

The final result is

$$\int_{\partial Z_k} d^2r \, v_{ki}(r) \left[\left(\alpha f_0 - \frac{1}{2} n \cdot D\nabla f_0\right)_{r_k^-} \right.$$

$$- \left.\left(\alpha f_0 + \frac{1}{2} n \cdot D\nabla f_0\right)_{r_k^+} \right]$$

$$+ \int_{Z_k} d^3r \, [D\nabla f_0 \cdot \nabla v_{ki} + v_{ki}(r)\sigma_a(r)f_0(r)]$$

$$= \int_{Z_k} d^3r \, v_{ki}(r)\sigma_s(r) \, [\phi_0^{(l+1/2)}(r) - \phi_0^{(l)}(r)] \ ,$$

$$1 \le i \le J_k, \ 1 \le k \le K \ . \quad (18)$$

[We emphasize that f_0 and ϕ_0 in this equation are our *approximate* solutions, as defined in Eqs. (12) and (17).] This equation defines a general DFE diffusion discretization on an arbitrary grid in Cartesian geometry. Note that the boundary condition is incorporated "naturally" into Eqs. (18), because we define

$$\left(\alpha f_0 + \frac{n \cdot D\nabla f_0}{2}\right)_{r_k^+} \equiv [1 - \beta(r)] \left(\alpha f_0 - \frac{n \cdot D\nabla f_0}{2}\right)_{r_k^-}$$

for r_k on problem boundary . (19)

That is, the incoming partial current on the problem boundary is taken to be the reflection of the outgoing partial current when $\beta = 0$ and zero when $\beta = 1$. (We note that other boundary conditions have been investigated for use in DSA schemes; see, for example, Ref. 11. Our choice seems natural to us, and it has always worked well for us.) We remark that the continuity of partial currents at cell interfaces is also incorporated "naturally" in system (18) because of definition (16).

The reader who is familiar with Khalil's DSA procedure[3] may wonder how the above procedure differs from Khalil's. After all, Khalil also begins with the continuous diffusion equation and discretizes it in a way that is similar to the way the transport equation was discretized. We explain this as follows. Khalil views transport discretizations as *balance* relations plus auxiliary *cell* relations, whereas we view our DFE transport discretization in terms of *weight functions* and *basis functions*. Khalil derives balance and cell relations for his diffusion discretization that closely resemble those of the given transport discretization; we derive a diffusion discretization that uses the same weight and basis functions as the transport discretization. That is, the features of the transport discretization that we try to mimic are not the same ones that Khalil tries to mimic. As a result, we obtain a different diffusion discretization and thus a different DSA method. (The theoretical performance of the two different DSA schemes is compared, for the linear discontinuous method in slab geometry, in Sec. V.)

IV.B. Second Derivation of Discontinuous Finite Element Diffusion

In this subsection, we derive our DFE diffusion discretization directly from the DFE transport discretization. This derivation is very different than the one just presented: Here we follow the upper-right path of Fig. 1, whereas before we followed the lower-left path. However, we shall obtain the same DFE diffusion equation. We include this subsection for two reasons. First, it shows the connection between our method and standard linear DSA, exposing the inconsistency between our diffusion and transport discretizations. We hope this will assist future researchers who attempt to develop inconsistent, but rapidly convergent, DSA

TABLE I

Comparison of Standard Linear DSA Procedure
Versus Our Modified Four-Step Procedure

Step	Description	
	Standard Linear DSA Procedure	Our Procedure
1a	Take zeroth angular moment of discretized transport equation.	Same
1b	Take first angular moment of discretized transport equation.	Same
2	Change iteration indices to $l + 1$ except on second and higher moment terms	Same, except do not change indices on certain zeroth- and first-moment terms.
3	Subtract acceleration equations from unaccelerated equations to reduce algebraic complexity.	Same
4	Eliminate first moments from resulting system, leaving a discretized diffusion equation for the scalar fluxes. May not be possible given high-order discretization schemes in two or three dimensions.	Same; always possible

methods. Second, we find it interesting that our two paths in Fig. 1 do lead to the same result.

We compare our procedure to that of standard linear DSA in Table I. The basic idea is to derive a diffusion discretization that is equivalent to the transport discretization when the transport angular flux is linearly anisotropic. This is what is meant by a "consistent" diffusion discretization. Standard linear DSA achieves this rigorously, while our procedure only approximates it.

Step (1a) of our procedure is to integrate the discretized transport equation, Eq. (13), over angle [i.e., operate with $\sum_m w_m(\cdot)$], giving

$$\int_{\partial Z_k} d^2r\, v_{ki}(\mathbf{r})\, [J_{outgoing}^{(l+1/2)}(\mathbf{r}_k^-) - J_{incoming}^{(l+1/2)}(\mathbf{r}_k^+)]$$

$$+ \int_{Z_k} d^3r\, [\phi_1^{(l+1/2)} \cdot \nabla v_{ki} + v_{ki}\sigma_t\phi_0^{(l+1/2)}]$$

$$= \int_{Z_k} d^3r\, v_{ki}[\sigma_s\phi_0^{(l)} + q_0] \ ,$$

$$1 \leq i \leq J_k, \ 1 \leq k \leq K \ . \quad (20)$$

Here we have included the iteration index l. We have also defined

$$J_{outgoing}^{(l+1/2)}(\mathbf{r}_k^-) \equiv \sum_{\mathbf{n}_k \cdot \mathbf{\Omega}_m > 0} w_m |\mathbf{n}_k \cdot \mathbf{\Omega}_m| \psi_m^{(l+1/2)}(\mathbf{r}_k^-) \ , \quad (21a)$$

$$J_{incoming}^{(l+1/2)}(\mathbf{r}_k^+) \equiv \sum_{\mathbf{n}_k \cdot \mathbf{\Omega}_m < 0} w_m |\mathbf{n}_k \cdot \mathbf{\Omega}_m| \psi_m^{(l+1/2)}(\mathbf{r}_k^+) \ , \quad (21b)$$

$$\phi_1^{(l+1/2)}(\mathbf{r}) \equiv \sum_m w_m \mathbf{\Omega}_m \psi_m^{(l+1/2)}(\mathbf{r}) \ , \quad (21c)$$

and we have noted that the surface integration and summation can be interchanged:

$$\sum_{all\ m} w_m \int_{[incoming\ \partial Z_k]_m} d^2r(\cdot)$$

$$= \int_{all\ \partial Z_k} d^2r \sum_{[incoming\ \Omega_m]_r} w_m(\cdot) \quad (22a)$$

and

$$\sum_{all\ m} w_m \int_{[outgoing\ \partial Z_k]_m} d^2r(\cdot)$$

$$= \int_{all\ \partial Z_k} d^2r \sum_{[outgoing\ \Omega_m]_r} w_m(\cdot) \ . \quad (22b)$$

We can expand angular fluxes in terms of moments, e.g.,

$$\psi_m = \phi_0 + 3\mathbf{\Omega}_m \cdot \phi_1 + h.o.t. \ , \quad (23)$$

where $h.o.t.$ means higher order angular-moment terms. When we expand the angular fluxes in Eqs. (21a) and (21b) and carry out the summations over m, we find

$$J_{outgoing}^{(l+1/2)}(\mathbf{r}_k^-) = \alpha\phi_0^{(l+1/2)}(\mathbf{r}_k^-) + \tfrac{1}{2}\mathbf{n}_k \cdot \phi_1^{(l+1/2)}(\mathbf{r}_k^-)$$
$$+ (h.o.t.)^{(l+1/2)} \quad (24a)$$

and

$$J_{incoming}^{(l+1/2)}(\mathbf{r}_k^+) = \alpha\phi_0^{(l+1/2)}(\mathbf{r}_k^+) - \tfrac{1}{2}\mathbf{n}_k \cdot \phi_1^{(l+1/2)}(\mathbf{r}_k^+)$$
$$+ (h.o.t.)^{(l+1/2)} \ , \quad (24b)$$

where we have assumed a symmetric quadrature that satisfies

$$\sum_{\mathbf{n} \cdot \mathbf{\Omega}_m > 0} w_m |\mathbf{n} \cdot \mathbf{\Omega}_m|^2 = \frac{1}{6} \quad (25a)$$

and defined

$$\alpha = \sum_{\mathbf{n} \cdot \mathbf{\Omega}_m > 0} w_m |\mathbf{n} \cdot \mathbf{\Omega}_m| \approx \frac{1}{4} \ . \quad (25b)$$

We note that as a consequence of transport boundary condition (13b), Eq. (24b) on problem boundaries becomes

$$J_{incoming}^{(l+1/2)}(r_k^+) \equiv \beta(r_k) \sum_{n \cdot \Omega_m < 0} w_m |n \cdot \Omega_m| \psi_m^{inc}(r_k)$$

$$+ [1 - \beta(r_k)] J_{outgoing}^{(l+1/2)}(r_k^-) \, ,$$

$$r_k \text{ on problem boundary .} \quad (26)$$

Thus, at the end of step 1a we have Eqs. (20) and definitions (24), (25), and (26). This is identical to standard linear DSA.

Step 1b of our procedure is to take the first angular moment of the DFE transport equation, Eq. (13); that is, to operate with $\Sigma_m w_m \Omega_m(\cdot)$. This produces an equation that relates scalar fluxes, currents, and higher order moments. After a bit of manipulation, this equation can be written as follows:

$$\int_{Z_k} d^3r \, v_{ki}(r) \left[\frac{2}{3} \nabla \cdot \Phi_2^{(l+1/2)} + \frac{1}{3} \nabla \phi_0^{(l+1/2)} \right.$$

$$\left. + \sigma_t \phi_1^{(l+1/2)} \right]$$

$$= \int_{Z_k} d^3r \, v_{ki}(r) q_1(r)$$

$$- \int_{\partial Z_k} d^2r \, v_{ki}(r) C^{(l+1/2)}(r) \, ,$$

$$1 \le i \le J_k, \ 1 \le k \le K \, , \quad (27)$$

where we have defined

$$C^{(l+1/2)}(r_k)$$

$$= \frac{n_k}{6} [\phi_0^{(l+1/2)}(r_k^+) - \phi_0^{(l+1/2)}(r_k^-)]$$

$$+ \frac{3}{16} [\phi_1^{(l+1/2)}(r_k^+) - \phi_1^{(l+1/2)}(r_k^-)]$$

$$+ \frac{3n_k}{16} n_k \cdot [\phi_1^{(l+1/2)}(r_k^+) - \phi_1^{(l+1/2)}(r_k^-)]$$

$$+ (h.o.t.)^{(l+1/2)} \, .$$

At this point, our procedure is still identical to standard linear DSA.

Step 2 of our procedure is to define acceleration equations by changing certain iteration indices to $(l+1)$ in Eqs. (20) through (27). We note that the standard linear DSA procedure leaves the iteration indices at $(l + \frac{1}{2})$ on terms involving second-and-higher angular moments, but updates all others to $(l + 1)$. This produces a consistent scheme. Our procedure is the same except that we leave the index at $(l + \frac{1}{2})$ on the term $C(r_k)$ that appears in Eq. (27). Because this term contains contributions from scalar fluxes and currents, our scheme is not consistent. Our result is

$$\int_{\partial Z_k} d^2r \, v_{ki}(r) [J_{outgoing}^{(l+1)}(r_k^-) - J_{incoming}^{(l+1)}(r_k^+)]$$

$$+ \int_{Z_k} d^3r [\phi_1^{(l+1)} \cdot \nabla v_{ki} + v_{ki} \sigma_t \phi_0^{(l+1)}]$$

$$= \int_{Z_k} d^3r \, v_{ki} [\sigma_s \phi_0^{(l+1)} + q_0] \, ,$$

$$1 \le i \le J_k, \ 1 \le k \le K \, , \quad (28)$$

$$J_{outgoing}^{(l+1)}(r_k^-) = \alpha \phi_0^{(l+1)}(r_k^-) + \frac{1}{2} n_k \cdot \phi_1^{(l+1)}(r_k^-)$$

$$+ (h.o.t.)^{(l+1/2)} \, , \quad (29a)$$

$$J_{incoming}^{(l+1)}(r_k^+)$$

$$= \begin{cases} \alpha \phi_0^{(l+1)}(r_k^+) - \frac{1}{2} n_k \cdot \phi_1^{(l+1)}(r_k^+) \\ \quad + (h.o.t.)^{(l+1/2)} \, , \\ \quad r_k \text{ not on problem boundary ,} \\ \beta(r_k) \sum_{n \cdot \Omega_m < 0} w_m |n \cdot \Omega_m| \psi_m^{inc}(r_k) \\ \quad + [1 - \beta(r_k)] J_{outgoing}^{(l+1/2)}(r_k^-) \, , \\ \quad r_k \text{ on problem boundary ,} \end{cases} \quad (29b)$$

and

$$\int_{Z_k} d^3r \, v_{ki}(r) \left[\frac{2}{3} \nabla \cdot \Phi_2^{(l+1/2)} + \frac{1}{3} \nabla \phi_0^{(l+1)} + \sigma_t \phi_1^{(l+1)} \right]$$

$$= \int_{Z_k} d^3r \, v_{ki}(r) q_1(r)$$

$$- \int_{\partial Z_k} d^2r \, v_{ki}(r) C^{(l+1/2)}(r) \, ,$$

$$1 \le i \le J_k, \ 1 \le k \le K \, . \quad (30)$$

Several things about Eqs. (28), (29), and (30) are worth noting. First, they are a coupled set of equations that completely determine the end-of-iteration scalar flux $\phi_0^{(l+1)}$ and current $\phi_1^{(l+1)}$. Second, Eq. (28) is a statement of zonewise conservation or "balance"; thus, the end-of-iteration scalar flux and current will satisfy zonal balance equations. Third, the end-of-iteration scalar flux and current depend only on known sources, second-and-higher moments, and $C^{(l+1/2)}$; thus, if the second-and-higher moments and $C^{(l+1/2)}$ terms are unimportant or if they are close to their converged values, the end-of-iteration scalar flux and current will be close to their converged values.

After step 2, our DSA method is fully defined. The remaining steps involve nothing but algebraic manipulation, the purpose of which is to put the equations into a form convenient for solution. Step 3 is to subtract the unaccelerated equations, Eqs. (20), (24), and (27), from the acceleration equations, Eqs. (28), (29),

and (30). The result is that all source terms, and all terms whose iteration indices are left at $(l + \frac{1}{2})$, subtract out. We thereby obtain equations for differences between $(l + 1)$'st iterates and $(l + \frac{1}{2})$'th iterates. Step 4 is to eliminate the first-moment terms from the system of equations, leaving a discretized diffusion equation for the scalar flux. This step may not be possible with standard linear DSA, because of the algebraic complexity introduced by requiring strict consistency.[2] However, it is always possible with our procedure, as we now demonstrate. If we define

$$f_0(r) = \phi_0^{(l+1)}(r) - \phi_0^{(l+1/2)}(r) \ , \tag{31a}$$

$$f_1(r) = \phi_1^{(l+1)}(r) - \phi_1^{(l+1/2)}(r) \ , \tag{31b}$$

and

$$\sigma_a(r) = \sigma_t(r) - \sigma_s(r) \ , \tag{31c}$$

then the difference between Eqs. (30) and (27) gives, after some manipulation, the following:

$$f_1(r) = -D\nabla f_0 \ , \tag{32}$$

where D is $1/(3\sigma_t)$. [In obtaining Eq. (32) we have assumed that gradients of our DFE basis functions reside in the function space spanned by the basis functions. This is true of most DFE methods.] If we use Eq. (32), then the differences between Eqs. (29) and (24) become

$$[J_{outgoing}^{(l+1)} - J_{outgoing}^{(l+1/2)}]_{r_k^-} = (\alpha f_0 - \frac{1}{2}n_k \cdot D\nabla f_0)_{r_k^-} \tag{33a}$$

and

$$[J_{incoming}^{(l+1)} - J_{incoming}^{(l+1/2)}]_{r_k^+} = \begin{cases} (\alpha f_0 + \frac{1}{2}n_k \cdot D\nabla f_0)_{r_k^+} \ , & r_k \text{ not on boundary} \ , \\ \gamma(r_k)[J_{outgoing}^{(l+1)} - J_{outgoing}^{(l+1/2)}]_{r_k^-} \ , & r_k \text{ on boundary} \ . \end{cases} \tag{33b}$$

Finally, if we use Eqs. (32) and (33), then the difference between Eqs. (28) and (20) gives

$$\int_{\partial Z_k} d^2 r \, v_{ki}(r) \left[\left(\alpha f_0 - \frac{1}{2} n \cdot D\nabla f_0 \right)_{r_k^-} - \left(\alpha f_0 + \frac{1}{2} n \cdot D\nabla f_0 \right)_{r_k^+} \right] + \int_{Z_k} d^3 r [D\nabla f_0 \cdot \nabla v_{ki} + v_{ki}(r)\sigma_a(r)f_0(r)]$$

$$= \int_{Z_k} d^3 r \, v_{ki}(r)\sigma_s(r)[\phi_0^{(l+1/2)}(r) - \phi_0^{(l)}(r)] \ , \quad 1 \leq i \leq J_k, \, 1 \leq k \leq K \ , \tag{34}$$

which is identical to the DFE diffusion equation that was derived by a completely different procedure in Sec. IV.A. We now see that, in the sense defined earlier, this equation is not consistent with DFE transport.

IV.C. Simple Case: Linear Discontinuous Finite Element, Slab Geometry

We now illustrate our DFE diffusion with the special case of the linear DFE in slab geometry, with specified incident flux on the left boundary and reflection on the right. The corresponding linear DFE transport discretization is described above in Eqs. (14). For this case, our diffusion discretization is

$$-\left[D \frac{df_0^{(l+1)}}{dx} \right]_{x_{k+1/2}} + \left[D \frac{df_0^{(l+1)}}{dx} \right]_{x_{k-1/2}} + \sigma_{ak} h_k f_{0k}^{(l+1)} = \sigma_{sk} h_k [\phi_{0k}^{(l+1/2)} - \phi_{0k}^{(l)}] \tag{35a}$$

and

$$-3\left[D \frac{df_0^{(l+1)}}{dx} \right]_{x_{k+1/2}} - 3\left[D \frac{df_0^{(l+1)}}{dx} \right]_{x_{k-1/2}} + 12 D_k \frac{f_{0k}^{x(l+1)}}{h_k} + \sigma_{ak} h_k f_{0k}^{x(l+1)} = \sigma_{sk} h_k [\phi_{0k}^{x(l+1/2)} - \phi_{0k}^{x(l)}] \ , \tag{35b}$$

where the net currents are defined in terms of partial currents:

$$\left(-D \frac{df_0}{dx} \right)_{x_{k+1/2}} = \begin{cases} 0 - \left[\alpha(f_{0k+1} - f_{0k+1}^x) + \dfrac{D_{k+1} f_{0k+1}^x}{h_{k+1}} \right] \ , & k = 0 \ , \\ \left[\alpha(f_{0k} + f_{0k}^x) - \dfrac{D_k f_{0k}^x}{h_k} \right] - \left[\alpha(f_{0k+1} - f_{0k+1}^x) + \dfrac{D_{k+1} f_{0k+1}^x}{h_{k+1}} \right] \ , & 0 < k < K \ , \\ 0 \ , & k = K \ . \end{cases} \tag{35c}$$

At this point, our slab geometry linear DFE diffusion discretization is completely specified by Eqs. (35). Note that a full DSA iteration consists of a transport sweep using Eqs. (14), the diffusion solution (35), and the addition of the diffusion solution f to the latest transport iterate $\phi^{(l+1/2)}$:

$$\phi_{0k}^{(l+1)} = \phi_{0k}^{(l+1/2)} + f_{0k}^{(l+1)}$$

and

$$\phi_{0k}^{x(l+1)} = \phi_{0k}^{x(l+1/2)} + f_{0k}^{x(l+1)} \quad . \tag{36}$$

In Appendix A, we illustrate our DFE diffusion discretization for curvilinear geometries using the example of linear elements in one-dimensional spherical geometries. In Appendix B, we provide a two-dimensional example, namely, the bilinear DFE scheme for rectangular spatial cells in Cartesian geometry. In Appendixes A and C, we demonstrate that our linear DFE schemes in one dimension can be manipulated into more conventional forms. In particular, we cast them as tridiagonal systems for either cell-averaged or cell-edge unknowns.

IV.D. Summary

We have given two distinctly different derivations of a DFE discretization of the diffusion equation, assuming an arbitrary spatial grid in Cartesian geometry. (We show in Appendix A that curvilinear geometries can be treated in much the same way.) The first derivation involves operating directly on the continuous diffusion equation and trying to mimic the transport discretization. This demonstrates the algebraic simplicity of our diffusion discretization. The second derivation involves operating on the DFE transport discretization with a modified version of the standard linear DSA procedure. This emphasizes the differences between our DSA and standard linear DSA, showing in particular that our DFE diffusion is not consistent with DFE transport. We shall show below that despite this "flaw," our scheme is unconditionally stable and rapidly convergent.

V. FOURIER ANALYSIS

In this section, we examine our DSA scheme applied to a simple model problem: an infinite homogeneous medium with constant cross sections and constant mesh spacing. We shall use a Fourier analysis that has become standard for such studies,[2,3,12] and consider both slab and x-y geometries.

V.A. Slab Geometry

We consider first the slab-geometry linear DFE system described earlier. We begin by subtracting iteration

equations (14), (35), and (36) from the same equations with the converged solution inserted. This leaves a set of equations describing the behavior of iteration errors:

$$\left[\frac{\mu_m}{h_k} (\hat{\psi}_{m,k+1/2} - \hat{\psi}_{m,k-1/2}) + \sigma_{tk} \hat{\psi}_{mk} \right]^{(l+1/2)}$$
$$= \sigma_{sk} \hat{\phi}_{0k}^{(l)} \quad , \tag{37a}$$

$$\left[\frac{3\mu_m}{h_k} (\hat{\psi}_{m,k+1/2} + \hat{\psi}_{m,k-1/2} - 2\hat{\psi}_{mk}) + \sigma_{tk} \hat{\psi}_{mk}^x \right]^{(l+1/2)}$$
$$= \sigma_{sk} \hat{\phi}_{0k}^{x(l)} \quad , \tag{37b}$$

$$\hat{\phi}_{0k}^{(l+1/2)} = \sum_{m=1}^{M} w_m \hat{\psi}_{mk}^{(l+1/2)} \quad ,$$

$$\hat{\phi}_{0k}^{x(l+1/2)} = \sum_{m=1}^{M} w_m \hat{\psi}_{mk}^{x(l+1/2)} \quad , \tag{37c}$$

$$\hat{\psi}_{m,k+1/2}^{(l+1/2)} = \begin{cases} \hat{\psi}_{mk}^{(l+1/2)} + \hat{\psi}_{mk}^{x(l+1/2)} \quad , & \mu_m > 0 \quad , \\ \hat{\psi}_{m,k+1}^{(l+1/2)} - \hat{\psi}_{m,k+1}^{x(l+1/2)} \quad , & \mu_m < 0 \quad , \end{cases} \tag{37d}$$

$$-\left[D \frac{d\hat{f}_0^{(l+1)}}{dx} \right]_{x_{k+1/2}} + \left[D \frac{d\hat{f}_0^{(l+1)}}{dx} \right]_{x_{k-1/2}}$$
$$+ \sigma_{ak} h_k \hat{f}_{0k}^{(l+1)} = \sigma_{sk} h_k [\hat{\phi}_{0k}^{(l+1/2)} - \hat{\phi}_{0k}^{(l)}] \quad , \tag{38a}$$

$$-3 \left[D \frac{d\hat{f}_0^{(l+1)}}{dx} \right]_{x_{k+1/2}} - 3 \left[D \frac{d\hat{f}_0^{(l+1)}}{dx} \right]_{x_{k-1/2}}$$
$$+ 12 D_k \frac{\hat{f}_{0k}^{x(l+1)}}{h_k} + \sigma_{ak} h_k \hat{f}_{0k}^{x(l+1)}$$
$$= \sigma_{sk} h_k [\hat{\phi}_{0k}^{x(l+1/2)} - \hat{\phi}_{0k}^{x(l)}] \quad , \tag{38b}$$

$$\left(-D \frac{d\hat{f}_0}{dx} \right)_{x_{k+1/2}} = \left[\alpha (\hat{f}_{0k} + \hat{f}_{0k}^x) - \frac{D_k \hat{f}_{0k}^x}{h_k} \right]$$
$$- \left[\alpha (\hat{f}_{0k+1} - \hat{f}_{0k+1}^x) \right.$$
$$\left. + \frac{D_{k+1} \hat{f}_{0k+1}^x}{h_{k+1}} \right] \quad , \tag{38c}$$

$$\hat{\phi}_{0k}^{(l+1)} = \hat{\phi}_{0k}^{(l+1/2)} + \hat{f}_{0k}^{(l+1)} \quad ,$$

and

$$\hat{\phi}_{0k}^{x(l+1)} = \hat{\phi}_{0k}^{x(l+1/2)} + \hat{f}_{0k}^{x(l+1)} \quad , \tag{39}$$

where the iteration errors are defined as follows:

$$[\hat{\psi}_{mk}, \hat{\phi}_{0k}, \hat{f}_{0k}]^{(l)} = [\psi_{mk}, \phi_{0k}, f_{0k}]^{(converged)}$$
$$- [\psi_{mk}, \phi_{0k}, f_{0k}]^{(l)}$$

and

$$[\hat{\psi}_{mk}^x, \hat{\phi}_{0k}^x, \hat{f}_{0k}^x]^{(l)} = [\psi_{mk}^x, \phi_{0k}^x, f_{0k}^x]^{(converged)}$$
$$- [\psi_{mk}^x, \phi_{0k}^x, f_{0k}^x]^{(l)} \quad . \tag{40}$$

For this analysis and throughout the remainder of this paper, we adopt definition (25b) for the parameter α unless otherwise stated.

Into Eqs. (37), (38), and (39), we insert the following Fourier ansatz:

$$\hat{\psi}_{mk}^{(l)} = \omega^l a_m e^{i\lambda x_k} \ , \quad i \equiv \sqrt{-1} \ , \tag{41a}$$

$$\hat{\psi}_{mk}^{x(l)} = \omega^l a_m^x e^{i\lambda x_k} \ , \tag{41b}$$

$$\hat{\phi}_{0k}^{(l)} = \omega^l A e^{i\lambda x_k} \ , \tag{41c}$$

$$\hat{\phi}_{0k}^{x(l)} = \omega^l A^x e^{i\lambda x_k} \ , \tag{41d}$$

$$\hat{f}_{0k}^{(l)} = \omega^l B e^{i\lambda x_k} \ , \tag{41e}$$

and

$$\hat{f}_{0k}^{x(l)} = \omega^l B^x e^{i\lambda x_k} \ . \tag{41f}$$

The result after considerable manipulation is a 2×2 matrix eigenvalue problem for the eigenvalues ω:

$$\omega v = [\mathbf{I} - \mathbf{L}]^{-1}[\mathbf{H} - \mathbf{L}]v \ . \tag{42}$$

The eigenvalues are factors by which various error modes are multiplied on each iteration. Hence, if all eigenvalues have magnitude less than unity, the iteration is unconditionally stable. The largest magnitude of all the eigenvalues is called the spectral radius; it determines the behavior of the iteration scheme after a sufficiently large number of iterations. A spectral radius of 0.1, for example, ensures that the magnitude of every error mode is reduced by at least a factor of 10 each iteration. We would like as small a spectral radius as possible; the smaller the spectral radius, the more rapidly the iterative scheme converges.

The matrices in Eq. (42), and hence the eigenvalues ω, depend on the quadrature set and on the parameters λh, $\sigma_t h$, and c, where c is the scattering ratio σ_s/σ_t. We have performed, for various quadrature sets and various values of the mesh spacing $\sigma_t h$, a numerical search for the maximum $|\omega|$ (i.e., the spectral radius) over all values of $c \in (0,1)$ and $\lambda h \in (0,\pi)$. We have found in every case that the maximum occurs as $c \to 1$, but that the value of λh at which the maximum occurs varies with $\sigma_t h$. Results are plotted for the S_2, S_4, S_8, and S_{16} cases in Fig. 2. For very fine mesh spacings, the spectral radius approaches that of the analytic (i.e., not discretized) equations—0.0 for S_2 and ≈ 0.2247 for S_{16}—which is what one expects. Further, we note that the spectral radius approaches zero (immediate convergence) for large mesh spacings. This could prove very important in applications such as radiative transfer, which require the use of very thick mesh spacings. Finally, we note that for intermediate mesh spacings of a few mean-free-paths, the spectral radius reaches a maximum ranging from $0.67c$ (S_2) to $0.50c$ (S_{16}).

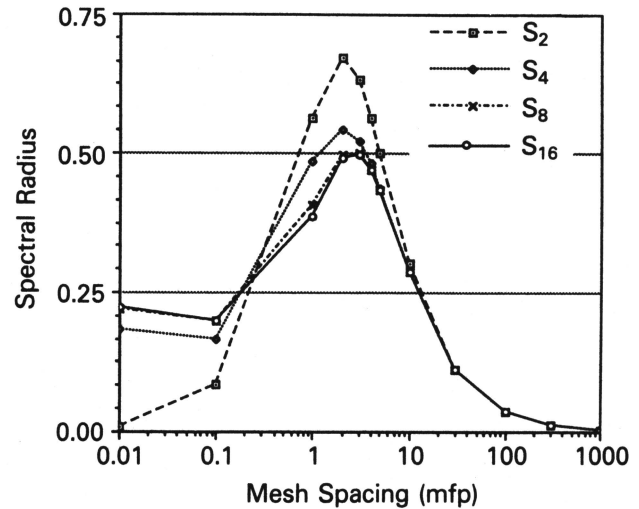For comparison, standard linear DSA for linear DFE in slab geometry has a spectral radius of 0.2247

Fig. 2. Slab geometry Fourier analysis results.

in the fine-mesh limit, rising to a maximum of 0.25 in the coarse-mesh limit.[2] The spectral radius of Khalil's DSA method for linear DFE in slab geometry has the same fine-mesh limit, but it decreases monotonically to 0.131 in the coarse-mesh limit.[3]

V.B. x-y Geometry

We have performed a similar analysis of the DSA method for bilinear DFE in two-dimensional Cartesian geometry. (This method is described in Appendix B.) As was the case in the slab-geometry analysis, we obtain equations describing the behavior of iteration errors. We then insert a Fourier ansatz of the form

$$E_{kj}^{(l)} = \omega^l \hat{E} e^{i(\lambda_x x_k - \lambda_y y_j)} \ , \quad i \equiv \sqrt{-1} \ , \tag{43}$$

where E denotes any of the iteration errors. The result is a matrix eigenvalue problem like Eq. (42), but this time the matrices are 4×4 (because we have four unknowns per zone), and they depend on the quadrature set, $(\lambda_x h^x)$, $(\lambda_y h^y)$, c, $\sigma_t h^x$, and $\sigma_t h^y$.

We have performed, for various values of $\sigma_t h^x$ and $\sigma_t h^y$, a numerical search for the maximum $|\omega|$ over all $c \in (0,1)$, $\lambda_x h^x \in (0,\pi)$, and $\lambda_y h^y \in (0,\pi)$. Thus, given particular values of c, $\sigma_t h^x$, and $\sigma_t h^y$, our computer code searches the plane $(0,\pi) \times (0,\pi)$ for a global extremum. (We note that this search is fairly difficult, because the global extrema are sometimes very sharp. We have taken pains to account for this, and we believe that the numbers reported here are accurate to the digits given.)

We have found in every case that the maximum $|\omega|$ occurs as $c \to 1$, but that the values of $\lambda_x h^x$ and $\lambda_y h^y$ at which the maximum occurs vary with $\sigma_t h^x$ and $\sigma_t h^y$. Results are given for several level-symmetric quadrature sets[13] in Tables II, III, and IV. These results

TABLE II

S_2 Level-Symmetric Quadrature Fourier Analysis Results, Two-Dimensional Cartesian Geometry

$\sigma\Delta x$	$\sigma\Delta y$								
	0.001	0.01	0.1	1.0	2.0	5.0	10.0	100	1000
0.001	0.50								
0.01	0.50	0.50							
0.1	0.48	0.48	0.47						
1.0	0.56	0.56	0.57	0.56					
2.0	0.67	0.67	0.67	0.67	0.67				
5.0	0.50	0.50	0.50	0.56	0.67	0.50			
10.0	0.30	0.30	0.30	0.56	0.67	0.50	0.30		
100.0	0.03	0.03	0.08	0.56	0.67	0.50	0.30	0.03	
1000.0	0.003	0.009	0.08	0.56	0.67	0.50	0.30	0.03	0.003

TABLE III

S_4 Level-Symmetric Quadrature Fourier Analysis Results, Two-Dimensional Cartesian Geometry

$\sigma\Delta x$	$\sigma\Delta y$								
	0.001	0.01	0.1	1.0	2.0	5.0	10.0	100	1000
0.001	0.25								
0.01	0.25	0.25							
0.1	0.23	0.25	0.23						
1.0	0.49	0.49	0.49	0.49					
2.0	0.55	0.55	0.55	0.55	0.55				
5.0	0.44	0.44	0.44	0.49	0.55	0.44			
10.0	0.28	0.28	0.28	0.49	0.55	0.44	0.28		
100.0	0.18	0.18	0.16	0.49	0.55	0.44	0.28	0.03	
1000.0	0.18	0.18	0.16	0.49	0.55	0.44	0.28	0.03	0.003

TABLE IV

S_8 Level-Symmetric Quadrature Fourier Analysis Results, Two-Dimensional Cartesian Geometry

$\sigma\Delta x$	$\sigma\Delta y$								
	0.001	0.01	0.1	1.0	2.0	5.0	10.0	100	1000
0.001	0.23								
0.01	0.23	0.23							
0.1	0.22	0.22	0.22						
1.0	0.42	0.42	0.42	0.42					
2.0	0.50	0.50	0.50	0.50	0.50				
5.0	0.43	0.43	0.43	0.43	0.50	0.43			
10.0	0.28	0.28	0.28	0.42	0.50	0.43	0.28		
100.0	0.22	0.22	0.20	0.42	0.50	0.43	0.28	0.04	
1000.0	0.22	0.22	0.20	0.42	0.50	0.43	0.28	0.03	0.003

are essentially the same as the slab-geometry results: The spectral radius peaks at $0.67c$ (S_2) or $\approx 0.5c$ (S_8) for intermediate mesh spacings, and it tends to zero for large mesh spacings. Again, we note that this thick-limit behavior could prove very important in some applications. In the fine-mesh limit, the spectral radius approaches that of the analytic (i.e., not discretized) DSA method for the discrete ordinates equations [0.500 for S_2, 0.228 for S_8 (Ref. 14)].

We note that the numerical estimates fall just below the analytical predictions. This is what we would expect, because these problems are finite and do not contain the full spectrum of error modes. We note further that the spherical-geometry results are essentially identical to the slab-geometry results. This is extremely encouraging, because we cannot Fourier-analyze the spherical-geometry method.

VI. NUMERICAL RESULTS

In this section, we present numerical results from several slab-geometry and spherical-geometry test problems. In all cases, we use the linear DFE method described in Sec. III.A (slabs) and Appendix A (spheres). We find that although the analysis described in Sec. V was limited to Cartesian geometries, infinite homogeneous media, and constant mesh spacing, its predictions appear to be upper bounds for slab and spherical geometries, heterogeneous media, and variable mesh spacings.

VI.A. Test Problem 1

Our first test problem is a simple homogeneous medium with constant cross sections, as shown in Fig. 3. We used the S_8 quadrature set to solve this problem given a variety of half-thicknesses and mesh spacings. We plot results for large half-thicknesses alongside the analysis predictions in Fig. 4, and we summarize all the results in Table V. We computed numerical estimates of the spectral radius ρ each iteration, using

$$\rho = \frac{\| \phi_0^{(l+1)} - \phi_0^{(l)} \|}{\| \phi_0^{(l)} - \phi_0^{(l-1)} \|} \ , \qquad (44)$$

where

$$\| f \| \equiv \left(\sum_j \Delta x_j f_j^2 \right)^{1/2} \ . \qquad (45)$$
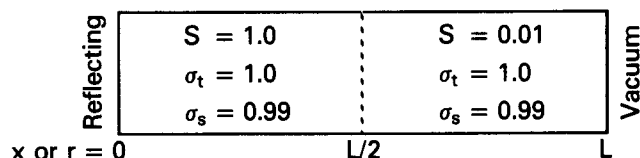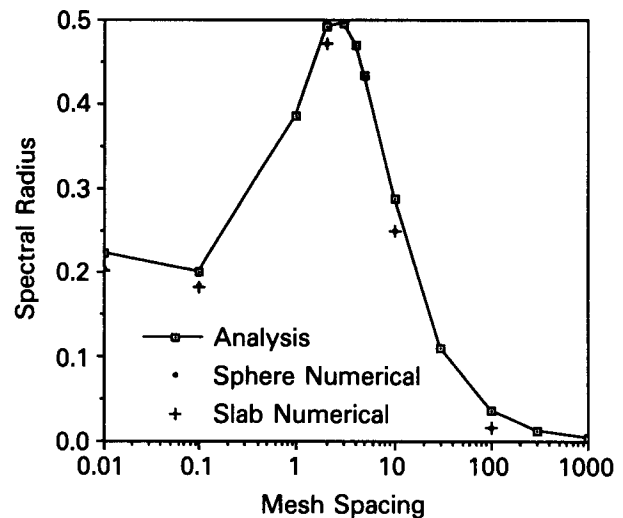
(The estimate from the final iteration appears in our tables.)

Fig. 4. Comparison of analysis results (slab geometry, S_8) against numerical results (slab and spherical geometries, S_8).

Fig. 3. Homogeneous test problem.

TABLE V

Results from Homogeneous Test Problem

Mesh Spacing	Half-Thickness	Iterations to 10^{-6}		Estimated Spectral Radius	
		Slab	Sphere	Slab	Sphere
0.01	30	7	7	0.203	0.205
0.1	10	7	7	0.175	0.183
	30	7	7	0.183	0.185
	100	7	7	0.183	0.184
2.0	30	13	13	0.472	0.468
	100	13	13	0.471	0.471
	300	13	13	0.471	0.471
10.0	100	10	10	0.249	0.248
	300	10	10	0.250	0.250
	1000	10	10	0.250	0.250
100.0	1000	4	4	0.017	0.017
	3000	4	4	0.017	0.017
	10000	4	4	0.017	0.017

| Reflecting | Region 1: Water
 S = 1.0
 σ_t = 3.3333
 σ_s = 3.3136 | Region 2: Water
 S = 0.0
 σ_t = 3.3333
 σ_s = 3.3136 | Region 3: Iron
 S = 0.0
 σ_t = 1.3333
 σ_s = 1.1077 | Region 4: Water
 S = 0.0
 σ_t = 3.3333
 σ_s = 3.3136 | Vacuum |

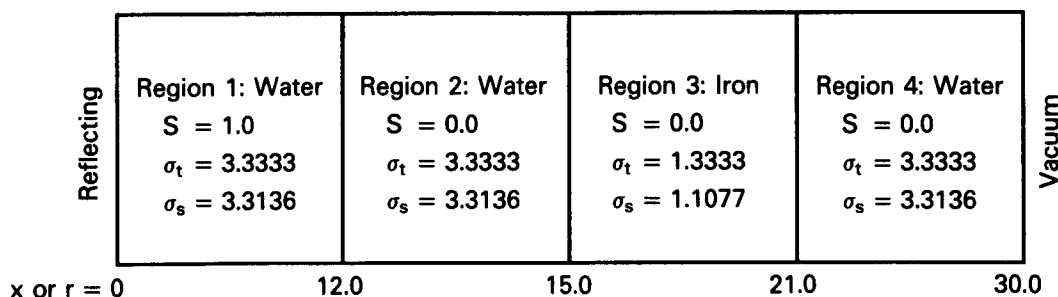x or r = 0   12.0   15.0   21.0   30.0

Fig. 5. Iron-water test problem.

We have run similar problems with other quadrature sets, with similar results. These results show that in a homogeneous slab or spherical medium, our DSA method is stable and rapidly convergent, performing at least as well as the analysis predicts.

VI.B. Test Problem 2

Our second problem is the more complicated "iron-water" test problem[2,3] depicted in Fig. 5. We note that this problem is heterogeneous and finite, and has variable mesh spacing. We present results generated with the S_8 Gauss-Legendre quadrature set in Table VI. We also show the "worst-case" cell thickness and the spectral radius predicted by our model-problem analysis (Sec. IV) for that thickness. (Here we define the worst-case thickness as the one that maximizes the model-problem spectral radius.) Once again, we see that numerical estimates of the spectral radius are bounded by the analytical predictions and that the spherical-geometry method behaves exactly like its slab-geometry counterpart.

We have run many other heterogeneous, variable-

TABLE VI

Results from Iron-Water Test Problem

Cells per Region	Iterations to 10^{-6}		Spectral Radius, Numerical Estimation		Worst-Case Cell Thickness (mfp)	Spectral Radius, Analytic Prediction
	Slab	Sphere	Slab	Sphere		
1	9	9	0.19	0.19	8	0.34
2	18	18	0.35	0.35	4	0.47
4	15	15	0.46	0.46	2	0.50
6	14	14	0.45	0.45	1.67	0.47
10	11	11	0.42	0.42	3	0.5
50	9	9	0.36	0.35	0.8	0.39
100	8	8	0.19	0.19	0.4	0.34
200	8	8	0.19	0.19	0.2	0.26

mesh problems, and we have always encountered similar results. Our results indicate that our DSA scheme is stable and rapidly convergent on all slab and spherical-geometry problems, with spectral radius bounded by the predictions of our model-problem Fourier analysis.

VII. CONCLUSIONS

We have presented a new discontinuous finite element discretization of the diffusion equation that can be used for diffusion synthetic acceleration of DFE transport iterations. We have performed Fourier analyses of simple DFE schemes on a simple model problem in one- and two-dimensional Cartesian geometries and have found that our method is unconditionally stable and rapidly convergent. We have also given numerical results in slab and spherical geometries; these results (and many others not shown) indicate that the predictions of the Fourier analysis are upper bounds even for non-Cartesian geometry, finite heterogeneous media, and variable mesh spacings.

In this paper, we have presented our methods and results only for "standard" DFE transport methods, essentially ignoring the interesting variations thereof that have been proposed recently.[15] We have in fact analyzed our DSA scheme for one of these variations in slab geometry (the $\theta = 1$ linear discontinuous method in the notation of Ref. 15) and found that its performance is essentially identical to that of the standard method discussed in this paper.

Our DSA method is characterized by a spectral radius that depends strongly on mesh spacing. For fine meshes, the spectral radius approaches the analytic (that is, not discretized) DSA result of $0.2247c$, where c is the scattering ratio. For mesh spacings of a few mean-free-paths, the spectral radius reaches a maximum of $0.67c$ for S_2 and a maximum less than $0.55c$ for other quadratures. As the mesh spacing increases further, the spectral radius decreases monotonically, approaching zero for thick mesh spacings, for all quadrature sets. The latter characteristic makes our DSA scheme seem attractive for applications such as

radiative transfer that involve optically thick, highly scattering cells. We note that this characteristic is not shared by other published DSA schemes, although it is shared by a different family of synthetic acceleration methods called "boundary-projection acceleration" methods.[12,16,17]

It is interesting that our method works even though our diffusion discretization is not strictly "consistent," in the usual sense, with the transport discretization. We hope that this information can be used in the future to help answer a fundamental question: What are the necessary and sufficient conditions that a diffusion discretization must meet in order to effectively accelerate a given transport scheme? In the early stages of DSA research, it appeared that strict consistency was both necessary and sufficient,[1,2] but this and other recent works have shown that it is not necessary.[3] However, we still do not know how much inconsistency a scheme can tolerate and remain effective. This is an important question, for the consistently differenced diffusion equation can be awkward to work with and potentially difficult to solve[2]; a bit of inconsistency could mean freedom to discretize the diffusion equation in a more easily solved form, which is of course crucial to the overall efficiency of the DSA scheme.

On the subject of efficiency, we show in Appendix C that in one-dimensional geometries our linear discontinuous diffusion equation can be cast as a three-point difference equation for either cell-averaged or cell-edge unknowns. Hence, in one dimension the diffusion solution involves solving a simple tridiagonal matrix equation. In two-dimensional geometries, we cannot produce a difference equation involving only one unknown per cell or vertex. Thus, the efficient solution of our DFE diffusion equations in two dimensions remains an open question. Morel and coworkers are currently addressing this question, investigating the multigrid method as a candidate for solving our bilinear DFE diffusion equations. Preliminary results are promising.[18]

Finally, we remark that our DFE diffusion discretization can be used to accelerate DFE transport eigenvalue iterations[19] and group-to-group scattering iterations as well as within-group iterations, in the same way that any linear DSA scheme can.

APPENDIX A

In this appendix, we derive our linear DFE diffusion discretization, which can be used to accelerate linear DFE transport iterations, in spherical geometry. We use the approach of Sec. III.A: Begin with the continuous diffusion equation, apply the DFE approximation to it, and treat cell-edge unknowns the same way they are treated in the DFE transport approximation. The purpose of this is to illustrate that our procedure is applicable to curvilinear geometries.

We begin with the spherical-geometry linear DFE discrete ordinates equations for one transport sweep:

$$\mu_m[r_{k+1/2}^2 \psi_{m,k+1/2}^{(l+1/2)} - r_{k-1/2}^2 \psi_{m,k-1/2}^{(l+1/2)}]$$

$$+ \sigma_{tk}[V_k \psi_{m,k}^{(l+1/2)} + W_k \psi_{m,k}^{x(l+1/2)}]$$

$$+ \frac{1}{w_m}\left\{ r_k \Delta r_k [(\gamma\psi)_{m+1/2k}^{(l+1/2)} - (\gamma\psi)_{m-1/2k}^{(l+1/2)}] \right.$$

$$\left. - \frac{\Delta r_k^2}{6}[(\gamma\psi)_{m+1/2k}^{x(l+1/2)} - (\gamma\psi)_{m-1/2k}^{x(l+1/2)}] \right\}$$

$$= V_k[\sigma_{sk}\phi_{0k}^{(l)} + q_{mk}] + W_k[\sigma_{sk}\phi_{0k}^{x(l)} + q_{mk}^x] ,$$

$$(A.1a)$$

$$\mu_m[r_{k+1/2}^2 \psi_{m,k+1/2}^{(l+1/2)} + r_{k-1/2}^2 \psi_{m,k-1/2}^{(l+1/2)}$$

$$- 2V_k \psi_{m,k}^{(l+1/2)} - 2W_k \psi_{m,k}^{x(l+1/2)}]$$

$$+ \frac{1}{w_m}\left\{ \frac{\Delta r_k^2}{6}[(\gamma\psi)_{m+1/2k}^{(l+1/2)} - (\gamma\psi)_{m-1/2k}^{(l+1/2)}] \right.$$

$$\left. - \frac{r_k \Delta r_k}{3}[(\gamma\psi)_{m+1/2k}^{x(l+1/2)} - (\gamma\psi)_{m-1/2k}^{x(l+1/2)}] \right\}$$

$$+ \sigma_{tk}[W_k \psi_{m,k}^{(l+1/2)} + X_k \psi_{m,k}^{x(l+1/2)}]$$

$$= W_k[\sigma_{sk}\phi_{0k}^{(l)} + q_{mk}] + X_k[\sigma_{sk}\phi_{0k}^{x(l)} + q_{mk}^x] ,$$

$$(A.1b)$$

$$\psi_{mk}^{(l+1/2)} = \tau_m \psi_{m+1/2k}^{(l+1/2)} + (1 - \tau_m)\psi_{m-1/2k}^{(l+1/2)} , \quad (A.2a)$$

$$\psi_{mk}^{x(l+1/2)} = \tau_m \psi_{m+1/2k}^{x(l+1/2)} + (1 - \tau_m)\psi_{m-1/2k}^{x(l+1/2)} , \quad (A.2b)$$

and

$$\psi_{m,k+1/2}^{(l+1/2)} = \begin{cases} \psi_{m,k}^{(l+1/2)} + \psi_{m,k}^{x(l+1/2)} , & \mu_m > 0 , \\ \psi_{m+1,k}^{(l+1/2)} - \psi_{m+1,k}^{x(l+1/2)} , & \mu_m < 0 , \end{cases} \quad (A.3)$$

where

$$V_k \equiv \int_{r_{k-1/2}}^{r_{k+1/2}} dr\, r^2 , \tag{A.4a}$$

$$W_k \equiv \int_{r_{k-1/2}}^{r_{k+1/2}} dr\, r^2 \frac{2(r - r_k)}{\Delta r_k} , \tag{A.4b}$$

$$X_k \equiv \int_{r_{k-1/2}}^{r_{k+1/2}} dr\, r^2 \left[\frac{2(r - r_k)}{\Delta r_k}\right]^2 , \tag{A.4c}$$

and

$$(\gamma\psi)_{m\pm 1/2,k}^{(l+1/2)} \equiv \gamma_{m\pm 1/2}\psi_{m\pm 1/2,k}^{(l+1/2)} . \tag{A.4d}$$

We obtained these equations by multiplying the spherical-geometry discrete ordinates equation by r^2 and by $2r^2(r - r_k)/\Delta r_k$, integrating the results over cell k, assuming a linear discontinuous approximation to the angular flux, and evaluating cell-edge quantities at the upstream side of each edge. The discrete ordinates equation assumed here is standard,[11] with weighted-diamond differencing in angle [see Eq. (A.2a)].

If we were accelerating a continuous transport iteration, our continuous diffusion acceleration equation would be

$$-\frac{1}{r^2}\frac{d}{dr}r^2 D \frac{df_0^{(l+1)}}{dr} + \sigma_a f_0^{(l+1)} = S \ , \quad (A.5a)$$

where

$$S(r) \equiv \sigma_s(r)[\phi_0^{(l+1/2)}(r) - \phi_0^{(l)}(r)] \ . \quad (A.5b)$$

Multiplying this diffusion equation by r^2 and by $2r^2(r - r_k)/\Delta r_k$, then integrating the results over cell k gives

$$-r^2 D \frac{df_0^{(l+1)}}{dr}\bigg|_{r_{k+1/2}} + r^2 D \frac{df_0^{(l+1)}}{dr}\bigg|_{r_{k-1/2}}$$
$$+ \sigma_{ak}[V_k f_{0k}^{(l+1)} + W_k f_{0k}^{x(l+1)}]$$
$$= V_k S_k + W_k S_k^x \quad (A.6a)$$

and

$$-r^2 D \frac{df_0^{(l+1)}}{dr}\bigg|_{r_{k+1/2}} - r^2 D \frac{df_0^{(l+1)}}{dr}\bigg|_{r_{k-1/2}}$$
$$+ \frac{4V_k D_k}{\Delta r_k^2} f_{0k}^{x(l+1)} + \sigma_{ak}[W_k f_{0k}^{(l+1)} + X_k f_{0k}^{x(l+1)}]$$
$$= W_k S_k + X_k S_k^x \ , \quad (A.6b)$$

where

$$f_{0k}^{(l+1)} \equiv \frac{1}{\Delta r_k}\int_{r_{k-1/2}}^{r_{k+1/2}} dr f_0^{(l+1)}(r) \quad (A.7a)$$

and

$$f_{0k}^{x(l+1)} \equiv \frac{1}{\Delta r_k}\int_{r_{k-1/2}}^{r_{k+1/2}} dr \frac{2(r - r_k)}{\Delta r_k} f_0^{(l+1)}(r) \ , \quad (A.7b)$$

and where we have made the linear discontinuous approximation

$$f^{(l+1)}(r) = f_{0k}^{(l+1)} + f_{0k}^{x(l+1)}\frac{2(r - r_k)}{\Delta r_k} \ . \quad (A.8)$$

Now we make the following definition for the cell-edge net currents:

$$-D \frac{df_0}{dr}\bigg|_{r_{k+1/2}} = J_{k+1/2}^+ - J_{k-1/2}^-$$

$$= \left(\alpha f_0 - \frac{D}{2}\frac{df_0}{dr}\right)_{r_{k+1/2-\epsilon}}$$
$$- \left(\alpha f_0 + \frac{D}{2}\frac{df_0}{dr}\right)_{r_{k+1/2+\epsilon}}$$

$$= \left[\alpha(f_{0k} + f_{0k}^x) - \frac{D_k f_{0k}^x}{\Delta r_k}\right]$$
$$- \left[\alpha(f_{0,k+1} - f_{0,k+1}^x)\right.$$
$$\left. + \frac{D_{k+1} f_{0,k+1}^x}{\Delta r_{k+1}}\right] \ . \quad (A.9)$$

Equations (A.6) and (A.9) constitute our linear DFE diffusion discretization for spherical geometry.

These equations can be combined, as was the case in slab geometry, to obtain a three-point difference equation for the cell-averaged values $\{\bar{f}_{0k}\}$:

$$-(d_{k+1/2}a_{k+1}^+)\bar{f}_{0,k+1}^{(l+1)}$$
$$+ (\sigma_{ak}V_k + d_{k+1/2}a_k^- + d_{k-1/2}a_k^+)\bar{f}_{0k}^{(l+1)}$$
$$- (d_{k-1/2}a_{k-1}^-)\bar{f}_{0,k-1}^{(l+1)}$$
$$= d_{k+1/2}(b_{k+1}^+ S_{k+1} - e_{k+1}^+ S_{k+1}^x)$$
$$+ d_{k-1/2}(b_{k-1}^- S_{k-1} + e_{k-1}^- S_{k-1}^x)$$
$$+ (V_k - d_{k+1/2}b_k^- - d_{k-1/2}b_k^+)S_k$$
$$+ (W_k - d_{k+1/2}e_k^- + d_{k-1/2}e_k^+)S_k^x \ , \quad (A.10)$$

where

$$\bar{f}_{0k}^{(l+1)} \equiv \frac{1}{V_k}\int_{r_{k-1/2}}^{r_{k+1/2}} dr\, r^2 f_0^{(l+1)}(r)$$
$$= f_{0k}^{(l+1)} + \frac{W_k}{V_k} f_{0k}^{x(l+1)} \ , \quad (A.11a)$$

$$a_k^\pm = \alpha - \sigma_{ak}\beta_k^\pm(V_k \mp W_k) \ , \quad (A.11b)$$

$$b_k^\pm = \beta_k^\pm(V_k \mp W_k) \ , \quad (A.11c)$$

$$e_k^\pm = \beta_k^\pm(X_k \mp W_k) \ , \quad (A.11d)$$

$$d_{k+1/2} = \frac{r_{k+1/2}^2}{1 + 2r_{k+1/2}^2(\beta_{k+1}^+ + \beta_k^-)} \ , \quad (A.11e)$$

and

$$\beta_k^\pm = \frac{\alpha\Delta r_k^2(V_k \pm W_k) - V_k\Delta r_k D_k}{4V_k^2 D_k + \sigma_{ak}\Delta r_k^2(V_k X_k - W_k^2)} \ . \quad (A.11f)$$

Upon solving this system for the $\{\bar{f}_{0k}\}$, we can easily recover the $\{f_{0k}^x\}$:

$$\left[\frac{4V_k^2 D_k + \sigma_{ak}\Delta r_k^2(V_k X_k - W_k^2)}{V_k\Delta r_k^2}\right]f_{0k}^{x(l+1)}$$

$$= (d_{k+1/2}a_{k+1}^+)\bar{f}_{0k+1}^{(l+1)} - (d_{k-1/2}a_{k-1}^-)\bar{f}_{0,k-1}^{(l+1)}$$

$$+ (d_{k-1/2}a_k^+ - d_{k+1/2}a_k^- - \sigma_{ak}W_k)\bar{f}_{0k}^{(l+1)}$$

$$+ (W_k - d_{k+1/2}b_k^- + d_{k-1/2}b_k^+)S_k$$

$$+ (X_k - d_{k+1/2}e_k^- - d_{k-1/2}e_k^+)S_k^x$$

$$+ d_{k+1/2}(b_{k+1}^+ S_{k+1} - e_{k+1}^+ S_{k+1}^x)$$

$$- d_{k-1/2}(b_{k-1}^- S_{k-1} + e_{k-1}^- S_{k-1}^x) , \quad (A.12)$$

and the $\{f_{0k}\}$:

$$f_{0k}^{(l+1)} = \bar{f}_{0k}^{(l+1)} - \frac{W_k}{V_k}f_{0k}^{x(l+1)} . \quad (A.13)$$

The next iterate can then be computed:

$$\phi_{0k}^{(l+1)} = \phi_{0k}^{(l+1/2)} + f_{0k}^{(l+1)} \quad (A.14a)$$

and

$$\phi_{0k}^{x(l+1)} = \phi_{0k}^{x(l+1/2)} + f_{0k}^{x(l+1)} . \quad (A.14b)$$

Hence, in spherical geometry our linear DFE diffusion discretization is given by Eqs. (A.10), (A.12), and (A.13). Our DSA scheme is given by these equations as well as Eqs. (A.1), (A.2), (A.3), and (A.14).

APPENDIX B

In this appendix, we give our bilinear DFE diffusion discretization for rectangular spatial cells in two-dimensional Cartesian geometry. This discretization can be used in a DSA scheme when the transport equation is discretized using the bilinear DFE method.

We begin by specifying the bilinear DFE discrete ordinates transport equations. We define

$$v_{kn1}(x,y) = b_{kn1}(x,y)$$

$$= \begin{cases} 1.0 , & x \in (x_{k-1/2}, x_{k+1/2}), \\ & y \in (y_{n-1/2}, y_{n+1/2}) , \\ 0, & \text{otherwise} , \end{cases}$$

$$v_{kn2}(x,y) = b_{kn2}(x,y)$$

$$= \begin{cases} \dfrac{2(x - x_k)}{h_k^x} , & x \in (x_{k-1/2}, x_{k+1/2}), \\ & y \in (y_{n-1/2}, y_{n+1/2}) , \\ 0 , & \text{otherwise} , \end{cases}$$

$$v_{kn3}(x,y) = b_{kn3}(x,y)$$

$$= \begin{cases} \dfrac{2(y - y_n)}{h_n^y} , & x \in (x_{k-1/2}, x_{k+1/2}), \\ & y \in (y_{n-1/2}, y_{n+1/2}) , \\ 0 , & \text{otherwise} , \end{cases}$$

$$v_{kn4}(x,y) = b_{kn4}(x,y)$$

$$= \begin{cases} \dfrac{2(x - x_k)}{h_k^x}\dfrac{2(y - y_n)}{h_n^y} , \\ \quad x \in (x_{k-1/2}, x_{k+1/2}), \\ \quad y \in (y_{n-1/2}, y_{n+1/2}) , \\ 0 , \qquad \text{otherwise} , \end{cases}$$

$$h_k^x = x_{k+1/2} - x_{k-1/2} ,$$

$$h_n^y = y_{n+1/2} - y_{n-1/2} ,$$

$$x_k = \tfrac{1}{2}(x_{k+1/2} + x_{k-1/2}) ,$$

$$y_n = \tfrac{1}{2}(y_{n+1/2} + y_{n-1/2}) ,$$

$$\mu_m = \mathbf{e}_x \cdot \mathbf{\Omega}_m = x \text{ component of } \mathbf{\Omega}_m ,$$

$$\eta_m = \mathbf{e}_y \cdot \mathbf{\Omega}_m = y \text{ component of } \mathbf{\Omega}_m ,$$

and

$$\psi_m(x,y) = \psi_{mkn} + \psi_{mkn}^x \frac{2(x - x_n)}{h_n^x}$$

$$+ \psi_{mkn}^y \frac{2(y - y_n)}{h_n^y}$$

$$+ \psi_{mkn}^{xy} \frac{2(x - x_k)}{h_k^x} \frac{2(y - y_n)}{h_n^y} ,$$

$$x \in (x_{k-1/2}, x_{k+1/2}), \; y \in (y_{n-1/2}, y_{n+1/2}) .$$

We assume for simplicity that the incident angular flux is specified on all boundaries. Then, inserting the above definitions into our generic DFE transport equations (13), we find that our bilinear DFE equations for a transport sweep are

$$\left[\frac{\mu_m}{h_k^x}(\psi_{m,k+1/2,n} - \psi_{m,k-1/2,n})\right.$$

$$+ \frac{\eta_m}{h_n^y}(\psi_{m,k,n+1/2} - \psi_{m,k,n-1/2})$$

$$\left.+ \sigma_{tkn}\psi_{mkn}\right]^{(l+1/2)} = \sigma_{skn}\phi_{0kn}^{(l)} + Q_{mkn} , \quad (B.1a)$$

$$\left[\frac{3\mu_m}{h_k^x}(\psi_{m,k+1/2n}+\psi_{m,k-1/2n}-2\psi_{mkn})\right.$$

$$+\frac{\eta_m}{h_n^y}(\psi_{m,k,n+1/2}^x-\psi_{m,k,n-1/2}^x)$$

$$\left.+\sigma_{tkn}\psi_{mkn}^x\right]^{(l+1/2)}=\sigma_{skn}\phi_{0kn}^{x(l)}+Q_{mkn}^x \ , \quad \text{(B.1b)}$$

$$\left[\frac{\mu_m}{h_k^x}(\psi_{m,k+1/2,n}^y-\psi_{m,k-1/2,n}^y)\right.$$

$$+\frac{3\eta_m}{h_n^y}(\psi_{m,k,n+1/2}+\psi_{m,k,n-1/2}-2\psi_{mkn})$$

$$\left.+\sigma_{tkn}\psi_{mkn}^y\right]^{(l+1/2)}=\sigma_{skn}\phi_{0kn}^{y(l)}+Q_{mkn}^y \ , \quad \text{(B.1c)}$$

$$\left[\frac{3\mu_m}{h_k^x}(\psi_{m,k+1/2,n}^y+\psi_{m,k-1/2,n}^y-2\psi_{mkj}^y)\right.$$

$$+\frac{3\eta_m}{h_n^y}(\psi_{m,k,n+1/2}^x+\psi_{m,k,n-1/2}^x-2\psi_{mkn}^x)$$

$$\left.+\sigma_{tkn}\psi_{mkn}^{xy}\right]^{(l+1/2)}=\sigma_{skn}\phi_{0kn}^{xy(l)}+Q_{mkn}^{xy} \ , \quad \text{(B.1d)}$$

$$\phi_{0kn}^{(l+1/2)}=\sum_{m=1}^{M}w_m\psi_{mkn}^{(l+1/2)} \ ,$$

$$\phi_{0kn}^{x(l+1/2)}=\sum_{m=1}^{M}w_m\psi_{mkn}^{x(l+1/2)} \ ,$$

$$\phi_{0kn}^{y(l+1/2)}=\sum_{m=1}^{M}w_m\psi_{mkn}^{y(l+1/2)} \ ,$$

and

$$\phi_{0kn}^{xy(l+1/2)}=\sum_{m=1}^{M}w_m\psi_{mkn}^{xy(l+1/2)} \ , \quad \text{(B.2)}$$

where

$$\psi_{m,k+1/2,n}^{(l+1/2)}=\begin{cases}\psi_{mkn}^{(l+1/2)}+\psi_{mkn}^{x(l+1/2)} \ , \\ \qquad \mu_m>0 \text{ and } k>0 \ , \\ \psi_{m,n}^{inc} \ , \quad \mu_m>0 \text{ and } k=0 \ , \\ \psi_{m,k+1,n}^{(l+1/2)}-\psi_{m,k+1,n}^{x(l+1/2)} \ , \\ \qquad \mu_m<0 \text{ and } k<k_{max} \ , \\ \psi_{m,n}^{inc} \ , \quad \mu_m<0 \text{ and } k=k_{max} \ , \end{cases} \quad \text{(B.3)}$$

$$\psi_{m,k+1/2,n}^{y(l+1/2)}=\begin{cases}\psi_{mkn}^{y(l+1/2)}+\psi_{mkn}^{xy(l+1/2)} \ , \\ \qquad \mu_m>0 \text{ and } k>0 \ , \\ \psi_{m,n}^{inc,y} \ , \quad \mu_m>0 \text{ and } k=0 \ , \\ \psi_{m,k+1,n}^{y(l+1/2)}-\psi_{m,k+1,n}^{xy(l+1/2)} \ , \\ \qquad \mu_m<0 \text{ and } k<k_{max} \ , \\ \psi_{m,n}^{inc,y} \ , \quad \mu_m<0 \text{ and } k=k_{max} \ , \end{cases} \quad \text{(B.4)}$$

$$\psi_{m,k,n+1/2}^{(l+1/2)}=\begin{cases}\psi_{mkn}^{(l+1/2)}+\psi_{mkn}^{y(l+1/2)} \ , \\ \qquad \eta_m>0 \text{ and } n>0 \ , \\ \psi_{m,k}^{inc} \ , \quad \eta_m>0 \text{ and } n=0 \ , \\ \psi_{m,k,n+1}^{(l+1/2)}-\psi_{m,k,n+1}^{y(l+1/2)} \ , \\ \qquad \eta_m<0 \text{ and } n<n_{max} \ , \\ \psi_{m,k}^{inc} \ , \quad \eta_m<0 \text{ and } n=n_{max} \ , \end{cases} \quad \text{(B.5)}$$

and

$$\psi_{m,k,n+1/2}^{x(l+1/2)}=\begin{cases}\psi_{mkn}^{x(l+1/2)}+\psi_{mkn}^{xy(l+1/2)} \ , \\ \qquad \eta_m>0 \text{ and } n>0 \ , \\ \psi_{m,k}^{inc,x} \ , \quad \eta_m>0 \text{ and } n=0 \ , \\ \psi_{m,k,n+1}^{x(l+1/2)}-\psi_{m,k,n+1}^{xy(l+1/2)} \ , \\ \qquad \eta_m<0 \text{ and } n<n_{max} \ , \\ \psi_{m,k}^{inc,x} \ , \quad \eta_m<0 \text{ and } n=n_{max} \ . \end{cases} \quad \text{(B.6)}$$

If we use the same definitions in our generic DFE diffusion equations (18) and (19), we obtain the following bilinear DFE diffusion discretization:

$$\frac{(J_{k+1/2,n}-J_{k-1/2,n})}{h_k^x}+\frac{(J_{k,n+1/2}-J_{k,n-1/2})}{h_n^y}$$

$$+\sigma_{akn}f_{0kn}=S_{0kn} \ , \quad \text{(B.7a)}$$

$$\frac{3(J_{k+1/2,n}+J_{k-1/2,n})}{h_k^x}+\frac{(J_{k,n+1/2}^x-J_{k,n-1/2}^x)}{h_n^y}$$

$$+\left[\sigma_{akn}+\frac{12D_{kn}}{(h_k^x)^2}\right]f_{0kn}^x=S_{0kn}^x \ , \quad \text{(B.7b)}$$

$$\frac{(J_{k+1/2,n}^y-J_{k-1/2,n}^y)}{h_k^x}+\frac{3(J_{k,n+1/2}+J_{k,n-1/2})}{h_n^y}$$

$$+\left[\sigma_{akn}+\frac{12D_{kn}}{(h_n^y)^2}\right]f_{0kn}^y=S_{0kj}^y \ , \quad \text{(B.7c)}$$

and

$$\frac{3(J^y_{k+1/2,n} + J^y_{k-1/2,n})}{h^x_k} + \frac{3(J^x_{k,n+1/2} + J^x_{k,n-1/2})}{h^y_n} + \left[\sigma_{akn} + \frac{12D_{kn}}{(h^x_k)^2} + \frac{12D_{kn}}{(h^y_n)^2}\right]f^{xy}_{0kn} = S^{xy}_{0kn} , \qquad (B.7d)$$

where, assuming vacuum boundaries, we have defined

$$J_{k+1/2,n} \equiv \begin{cases} -\left[\alpha(f_{0,k+1,n} - f^x_{0,k+1,n}) + \left(\frac{D}{h^x} f^x_0\right)_{k+1,n}\right] , & k = 0 , \\ \alpha(f_{0kn} + f^x_{0kn} - f_{0,k+1,n} + f^x_{0,k+1,n}) - \left(\frac{D}{h^x} f^x_0\right)_{kn} - \left(\frac{D}{h^x} f^x_0\right)_{k+1,n} , & 0 < k < k_{max} , \quad (B.8) \\ \left[\alpha(f_{0kn} + f^x_{0kn}) - \left(\frac{D}{h^x} f^x_0\right)_{kn}\right] , & k = k_{max} , \end{cases}$$

$$J^y_{k+1/2,n} \equiv \begin{cases} -\left[\alpha(f^y_{0,k+1,n} - f^{xy}_{0,k+1,n}) + \left(\frac{D}{h^x} f^{xy}_0\right)_{k+1,n}\right] , & k = 0 , \\ \alpha(f^y_{0kn} + f^{xy}_{0kn} - f^y_{0,k+1,n} + f^{xy}_{0,k+1,n}) - \left(\frac{D}{h^x} f^{xy}_0\right)_{kn} - \left(\frac{D}{h^x} f^{xy}_0\right)_{k+1,n} , & 0 < k < k_{max} , \quad (B.9) \\ \left[\alpha(f^y_{0kn} + f^{xy}_{0kn}) - \left(\frac{D}{h^x} f^{xy}_0\right)_{kn}\right] , & k = k_{max} , \end{cases}$$

$$J_{k,n+1/2} \equiv \begin{cases} -\left[\alpha(f_{0,k,n+1} - f^y_{0,k,n+1}) + \left(\frac{D}{h^y} f^y_0\right)_{k,n+1}\right] , & n = 0 , \\ \alpha(f_{0kn} + f^y_{0kn} - f_{0,k,n+1} + f^y_{0,k,n+1}) - \left(\frac{D}{h^y} f^y_0\right)_{kn} - \left(\frac{D}{h^y} f^y_0\right)_{k,n+1} , & 0 < n < n_{max} , \quad (B.10) \\ \left[\alpha(f_{0kn} + f^y_{0kn}) - \left(\frac{D}{h^y} f^y_0\right)_{kn}\right] , & n = n_{max} , \end{cases}$$

and

$$J^x_{k,n+1/2} \equiv \begin{cases} -\left[\alpha(f^x_{0,k,n+1} - f^{xy}_{0,k,n+1}) + \left(\frac{D}{h^y} f^{xy}_0\right)_{k,n+1}\right] , & n = 0 , \\ \alpha(f^x_{0kn} + f^{xy}_{0kn} - f^x_{0,k,n+1} + f^{xy}_{0,k,n+1}) - \left(\frac{D}{h^y} f^{xy}_0\right)_{kn} - \left(\frac{D}{h^y} f^{xy}_0\right)_{k,n+1} , & 0 < n < n_{max} , \quad (B.11) \\ \left[\alpha(f^x_{0kn} + f^{xy}_{0kn}) - \left(\frac{D}{h^y} f^{xy}_0\right)_{kn}\right] , & n = n_{max} . \end{cases}$$

We have not explored efficient solution methods for this system of equations. We cannot obtain a simple zone-centered or point-centered difference equation, as we could in one dimension. We therefore must state that efficient solution of our DFE diffusion system in two dimensions remains an open question.

APPENDIX C

In this appendix, we demonstrate that our linear DFE diffusion equations in slab geometry can be manipulated into somewhat conventional forms, namely,

tridiagonal systems for cell-averaged or cell-edge unknowns. We begin with the cell-averaged system. If we add Eq. (35a) to one-third of Eq. (35b), we obtain

$$-2\left[D \frac{df^{(l+1)}_0}{dx}\right]_{x_{k+1/2}} + \sigma_{ak} h_k f^{(l+1)}_{0k}$$

$$+ \left(\frac{\sigma_{ak} h_k}{3} + \frac{4D_k}{h_k}\right)f^{x(l+1)}_{0k}$$

$$= h_k\left(S^{(l+1/2)}_{0k} + \frac{S^{x(l+1/2)}_{0k}}{3}\right) , \qquad (C.1)$$

where we have defined the shorthand notation

$$S_{0k}^{(l+1/2)} = \sigma_{sk}[\phi_{0k}^{(l+1/2)} - \phi_{0k}^{(l)}]$$

and

$$S_{0k}^{x(l+1/2)} = \sigma_{sk}[\phi_{0k}^{x(l+1/2)} - \phi_{0k}^{x(l)}] \ .$$

If we subtract one-third of Eq. (35b) from Eq. (35a), with both equations written for cell $k + 1$, we obtain

$$2\left[D\frac{df_0^{(l+1)}}{dx}\right]_{x_{k+1/2}} + \sigma_{ak+1}h_{k+1}f_{0k+1}^{(l+1)} - \left(\frac{\sigma_{ak+1}h_{k+1}}{3} + \frac{4D_{k+1}}{h_{k+1}}\right)f_{0k+1}^{x(l+1)} = h_{k+1}\left[S_{0k+1}^{(l+1/2)} - \frac{S_{0k+1}^{x(l+1/2)}}{3}\right] \ . \quad (C.2)$$

We solve Eq. (C.1) for f_{0k+1}^x and Eq. (C.2) for f_{0k}^x, then insert the results into Eq. (35c) and manipulate to obtain

$$-D\frac{df_0^{(l+1)}}{dx}\bigg|_{x_{k+1/2}} = -d_{k+1/2}(a_{k+1}f_{0k+1} - a_kf_{0k})^{(l+1)}$$

$$- d_{k+1/2}\left[b_{k+1}\left(S_{0k+1} - \frac{S_{0k+1}^x}{3}\right) - b_k\left(S_{0k} + \frac{S_{0k}^x}{3}\right)\right]^{(l+1/2)} \ , \quad (C.3)$$

where

$$d_{k+1/2} = \frac{1}{1 + 2\beta_k + 2\beta_{k+1}} \ , \quad (C.4a)$$

$$a_k = \alpha - \beta_k\sigma_{ak}h_k \ , \quad (C.4b)$$

$$b_k = \beta_k h_k \ , \quad (C.4c)$$

and

$$\beta_k = \frac{3(\alpha h_k - D_k)}{12D_k + \sigma_{ak}h_k^2} \ . \quad (C.4d)$$

Finally, we insert the expression (C.3) for the net current into the balance equation (35a) to produce the desired three-point relation:

$$-(d_{k+1/2}a_{k+1})f_{0k+1}^{(l+1)} + [(d_{k+1/2} + d_{k-1/2})a_k + \sigma_{ak}h_k]f_{0k}^{(l+1)} - (d_{k-1/2}a_{k-1})f_{0k-1}^{(l+1)}$$

$$= \left[(d_{k+1/2}b_{k+1})\left(S_{0k+1} - \frac{S_{0k+1}^x}{3}\right) + (d_{k-1/2}b_{k-1})\left(S_{0k-1} + \frac{S_{0k-1}^x}{3}\right)\right]^{(l+1/2)}$$

$$- \left\{[(d_{k+1/2} + d_{k-1/2})b_k - h_k]S_{0k} + [(d_{k+1/2} - d_{k-1/2})b_k]\frac{S_{0k}^x}{3}\right\}^{(l+1/2)} \ . \quad (C.5)$$

Once this tridiagonal system is solved for the $\{f_{0k}\}$, the $\{f_{0k}^x\}$ are easily obtained (with only local information) using

$$\left(\frac{12D_k + \sigma_{ak}h_k^2}{3h_k}\right)f_{0k}^{x(l+1)} = d_{k+1/2}\left\{a_{k+1}f_{0k+1}^{(l+1)} + b_{k+1}\left[S_{0k+1}^{(l+1/2)} - \frac{S_{0k+1}^{x(l+1/2)}}{3}\right]\right\}$$

$$- (d_{k+1/2} - d_{k-1/2})[a_kf_{0k}^{(l+1)} + b_kS_{0k}^{(l+1/2)}]$$

$$+ (\sigma_{sk}h_k - d_{k+1/2} - d_{k-1/2})\left[\frac{S_{0k}^{x(l+1/2)}}{3}\right]$$

$$+ d_{k-1/2}\left\{a_{k-1}f_{0k-1}^{(l+1)} + b_{k-1}\left[S_{0k-1}^{(l+1/2)} + \frac{S_{0k-1}^{x(l+1/2)}}{3}\right]\right\} \ . \quad (C.6)$$

We derived this relation using Eqs. (C.3), (C.1), and (35b).

We turn next to manipulating our linear discontinuous diffusion equation into a three-point difference equation whose unknowns are centered at cell edges. To do this, we define cell-edge scalar fluxes to be twice the sum of the cell-edge partial currents. If we assume a vacuum boundary at the left and a reflecting boundary at the right, this gives

$$f_{0,k+1/2} \equiv \begin{cases} 2\left(\alpha f_{0k+1} - \alpha f^x_{0k+1} + \dfrac{D_{k+1}}{h_{k+1}} f^x_{0k+1}\right) , & k = 0 , \\[2em] 2\alpha(f_{0k} + f^x_{0k} + f_{0,k+1} - f^x_{0,k+1}) - 2\dfrac{D_k}{h_k} f^x_{0k} + 2\dfrac{D_{k+1}}{h_{k+1}} f^x_{0,k+1} , & 0 < k < K , \\[2em] 4\left(\alpha f_{0k} + \alpha f^x_{0k} - \dfrac{D_k}{h_k} f^x_{0k}\right) , & k = K . \end{cases} \qquad (C.7)$$

Note that this is consistent with Eq. (35c), which defines cell-edge net currents to be the difference between cell-edge partial currents. Equations (35c) and (C.1) immediately produce

$$(\sigma_{ak}h_k + 4\alpha)f_{0k} + \left(\frac{\sigma_{ak}h_k}{3} + 4\alpha\right)f^x_{0k}$$

$$= f_{0,k+1/2} + h_k\left(S_k + \frac{S^x_k}{3}\right) , \qquad (C.8)$$

while Eqs. (35c) and (C.2), with (C.2) written for cell k, immediately produce

$$(\sigma_{ak}h_k + 4\alpha)f_{0k} - \left(\frac{\sigma_{ak}h_k}{3} + 4\alpha\right)f^x_{0k}$$

$$= f_{0,k-1/2} + h_k\left(S_k - \frac{S^x_k}{3}\right) . \qquad (C.9)$$

We add and subtract Eqs. (C.8) and (C.9) to obtain expressions for f_{0k} and f^x_{0k} in terms of the edge fluxes and sources:

$$f_{0k} = \left(\frac{1}{\sigma_{ak}h_k + 4\alpha}\right)\left(\frac{f_{0,k+1/2} + f_{0,k-1/2}}{2} + h_kS_k\right)$$

$$(C.10a)$$

and

$$f^x_{0k} = \left(\frac{1}{\frac{1}{3}\sigma_{ak}h_k + 4\alpha}\right)$$

$$\times \left(\frac{f_{0,k+1/2} - f_{0,k-1/2}}{2} + \frac{1}{3}h_kS_k\right) . \qquad (C.10b)$$

We insert these expressions into Eqs. (C.1) and (C.2) and add the results to obtain our edge-differenced diffusion equation:

$$-d_{k+1}(f_{0,k+3/2} - f_{0,k+1/2}) + d_k(f_{0,k+1/2} - f_{0,k-1/2})$$

$$+ a_{k+1}f_{0,k+3/2} + (a_{k+1} + a_k)f_{0,k+1/2}$$

$$+ a_kf_{0,k-1/2}$$

$$= \frac{4\alpha}{4\alpha + \sigma_{ak}h_k} h_kS_k + \frac{4\alpha}{4\alpha + \sigma_{ak+1}h_{k+1}} h_{k+1}S_{k+1}$$

$$+ \frac{4\alpha}{4\alpha + \frac{1}{3}\sigma_{ak}h_k} h_kS^x_k$$

$$- \frac{4\alpha}{4\alpha + \frac{1}{3}\sigma_{ak+1}h_{k+1}} h_{k+1}S^x_{k+1} , \qquad (C.11)$$

where

$$d_k = \frac{\sigma_{ak}h^2_k + 12D_k}{2\sigma_{ak}h^2_k + 24\alpha h^2_k}$$

and

$$a_k = \frac{\sigma_{ak}h_k}{2\sigma_{ak}h_k + 8\alpha} . \qquad (C.12)$$

Once this tridiagonal system is solved for the $\{f_{0,k+1/2}\}$, the $\{f_{0k}\}$ and $\{f^x_{0k}\}$ are easily obtained via Eqs. (C.10).

ACKNOWLEDGMENTS

REFERENCES

1. R. E. ALCOUFFE, Nucl. Sci. Eng., 64, 344 (1977).

2. E. W. LARSEN, Nucl. Sci. Eng., 82, 47 (1982).

3. H. KHALIL, Nucl. Sci. Eng., 98, 226 (1988).

4. J. E. MOREL, Nucl. Sci. Eng., 82, 34 (1982).

5. J. AULL, "Acceleration of the Inner Iteration of the DOT-IV Transport Code Using a New Source Correction Scheme," ORNL/TM-7404, Oak Ridge National Laboratory (1980).

6. E. W. LARSEN and R. E. ALCOUFFE, "The Linear Characteristic Method for Spatially Discretizing the Discrete-Ordinates Equations in x, y-Geometry," Proc. Int. Conf. Advances in Mathematical Methods for the Solution of Nuclear Engineering Problems, Munich, FRG, April 27-29, 1981, Vol. 1, p. 99, Kernforschungszentrum Karlsruhe (1981).

7. W. H. REED, *Nucl. Sci. Eng.*, **45**, 245 (1971).

8. R. E. ALCOUFFE, E. W. LARSEN, W. F. MILLER, Jr., and B. R. WIENKE, *Nucl. Sci. Eng.*, **71**, 111 (1979).

9. M. L. ADAMS and W. R. MARTIN, *Trans. Am. Nucl. Soc.*, **54**, 159 (1987).

10. W. R. MARTIN and J. J. DUDERSTADT, *Nucl. Sci. Eng.*, **62**, 371 (1977).

11. D. VALOUGEORGIS, *Nucl. Sci. Eng.*, **100**, 142 (1988).

12. M. L. ADAMS and W. R. MARTIN, *Nucl. Sci. Eng.*, **100**, 177 (1988).

13. E. E. LEWIS and W. F. MILLER, Jr., *Computational Methods of Neutron Transport*, John Wiley & Sons, New York (1984).

14. M. L. ADAMS, "Diffusion-Synthetic Acceleration of Discrete-Ordinates Iterations: The Fine-Mesh Limit," in preparation.

15. E. W. LARSEN and J. E. MOREL, *J. Comput. Phys.*, **83**, 212 (1989).

16. R. D. LAWRENCE, *Trans. Am. Nucl. Soc.*, **53**, 280 (1986).

17. M. L. ADAMS and W. R. MARTIN, *Trans. Am. Nucl. Soc.*, **53**, 282 (1986).

18. J. E. MOREL, Los Alamos National Laboratory, Private Communication (1991).

19. M. L. ADAMS and E. W. LARSEN, "Linear Diffusion-Synthetic Acceleration of k-Eigenvalue Problems," *Proc. Int. Conf. Advances in Nuclear Engineering Computation and Radiation Shielding*, Santa Fe, New Mexico, April 9-13, 1989.